

Viscoelasticity and Rubber Elasticity

At the extremes, a polymer may exhibit mechanical behavior characteristic of either an elastic solid or a viscous liquid. The actual response depends upon temperature, in relation to the glass-transition temperature (T_g) of the polymer, and upon the time scale of the deformation. Under usual circumstances, the mechanical response of polymeric materials will be intermediate between that of an ideal elastic or viscous liquid. In other words, polymers are *viscoelastic*. This behavior is readily illustrated by Silly Putty, which is a silicone rubber having a low T_g . If rolled up into a ball and dropped to the floor, it will bounce with the resilience of a rubber ball. This is a manifestation of elastic behavior resulting from rapid deformation. If left on a desk for several days, the ball will flatten—it will flow like a viscous liquid over a long time. If pulled at a moderate rate of strain, the ball will elongate with high extension and eventually fail. This chapter seeks to develop the fundamental concepts of polymer viscoelasticity and rubber elasticity and to describe the basic experimental methods used to study these properties.

5.1 Introduction to Viscoelasticity

Viscoelastic behavior may be characterized by a variety of techniques that record the time-dependent response of a polymeric solid, melt, or solution to a periodic perturbation such as the application of a sinusoidal strain or an electrical voltage. The most commonly used method to measure viscoelastic properties as a function of temperature and time (frequency) is dynamic-mechanical analysis, which records the stress response to an application of a sinusoidal strain. In comparison, dielectric methods record the temperature and frequency dependence of the dielectric constant to an oscillatory voltage applied to a sample pressed between two electrodes. The basic principles of dynamic-mechanical and dielectric analysis and the experimental methods used to measure dynamic-mechanical and dielectric properties of polymers are presented in the following sections.

5.1.1 Dynamic-Mechanical Analysis

In dynamic testing, the stress is measured as a function of strain that is some periodic function of time, usually a sine wave. Unlike fatigue tests (see Section 4.4.2), dynamic-mechanical properties are measured at low strain such that deformation is not permanent. Commercial dynamic-testing instruments are available for operation in several modes of deformation (e.g., tensile, torsion, compression, flexure, and shear) and over several decades of frequencies. The principles of dynamic-mechanical analysis are described next.

Theory. For a tensile strain that is a sinusoidal function of time, t , the strain function may be expressed as

$$\varepsilon = \varepsilon^{\circ} \sin(\omega t). \quad (5.1)$$

In this expression, ε° is the amplitude of the applied strain and ω is the angular frequency of oscillation (units of radians per second). The *angular* frequency is related to frequency, f , measured in cycles per second (Hz), as $\omega = 2\pi f$. The usual range of frequencies for dynamic-mechanical experiments is 0.1 to 110 Hz (0.628 to 691 rad s⁻¹).

The stress resulting from the applied sinusoidal strain will also be a sinusoidal function, which may be written in the most general form as

$$\sigma = \sigma^{\circ} \sin(\omega t + \delta) \quad (5.2)$$

where σ° is the amplitude of the stress response and δ is the *phase angle* between the stress and the strain, as illustrated by Figure 5-1. The phase angle is a measure of the viscous response of the material to dynamic strain as discussed later.

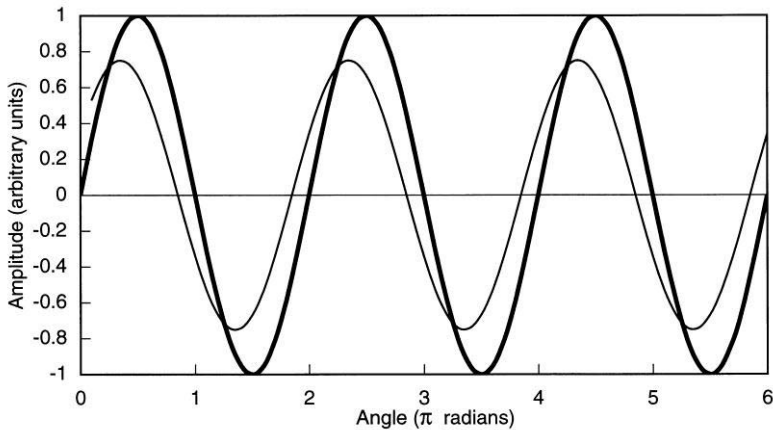


Figure 5-1 Representation of an arbitrary strain function (thick line) and resulting stress response (thin line) of a viscoelastic material. In this example, the stress is out of phase with the strain by 45° (i.e., $\delta = \pi/4$ radians), and its amplitude is arbitrarily set at 75% of the strain amplitude (i.e., $\sigma^0/\varepsilon^0 = 0.75$).

In the case of an ideal elastic solid, the stress is always in phase with strain (i.e., $\delta = 0$ in eq. (5.2)). This can be shown from substitution of eq. (5.1) into Hooke's law (eq. 4.46)

$$\sigma = E\varepsilon = E\varepsilon^0 \sin(\omega t) = \sigma^0 \sin(\omega t) \quad (5.3)$$

where σ^0 is the magnitude (i.e., $\sigma^0 = E\varepsilon^0$) of the resulting stress function.

In contrast, the stress of an ideal viscous fluid is always 90° out of phase (i.e., $\delta = \pi/2$) with the strain. This can be shown to result from Newton's law of viscosity, given as

$$\boxed{\sigma = \eta \left(\frac{d\varepsilon}{dt} \right)}. \quad (5.4)$$

The derivative of ε , given by eq. (5.1), with respect to time is

$$\frac{d\varepsilon}{dt} = \omega \varepsilon^0 \cos(\omega t). \quad (5.5)$$

Substitution of this expression into eq. (5.4), and noting that the cosine function is 90° out of phase with the sine function, gives

$$\sigma = \eta \omega \varepsilon^0 \cos(\omega t) = \sigma^0 \sin\left(\omega t + \frac{\pi}{2}\right) \quad (5.6)$$

where

$$\sigma^o = \eta\omega\varepsilon^o. \quad (5.7)$$

At temperatures below T_g , polymeric materials behave more as Hookean solids at small deformations, but at higher temperatures (i.e., in the vicinity of T_g) their behavior is distinctly viscoelastic. Over these temperatures, δ will have a (temperature-dependent) value between 0° (totally elastic) and 90° (totally viscous).

An alternative, and perhaps more useful, approach to discussing the dynamic response of a viscoelastic material to an applied cyclical strain is by use of complex number notation by which a complex strain, ε^* , can be represented as

$$\varepsilon^* = \varepsilon^o \exp(i\omega t) \quad (5.8)$$

where $i = \sqrt{-1}$. Following the form of eq. (5.2), the resulting complex stress, σ^* , can be written as

$$\sigma^* = \sigma^o \exp[i(\omega t + \delta)]. \quad (5.9)$$

It follows from Hooke's law that a *complex modulus*, E^* , can be defined as the ratio of complex stress to complex strain as

$$E^* = \frac{\sigma^*}{\varepsilon^*} = \left(\frac{\sigma^o}{\varepsilon^o} \right) \exp(i\delta). \quad (5.10)$$

This complex modulus can be resolved into two components—one that is in phase (i.e., E') and one that is out of phase (i.e., E'') with the applied strain. Substitution of *Euler's identity*

$$\exp(i\delta) = \cos\delta + i\sin\delta \quad (5.11)$$

into eq. (5.10) gives

$$E^* = \left(\frac{\sigma^o}{\varepsilon^o} \right) \cos\delta + i \left(\frac{\sigma^o}{\varepsilon^o} \right) \sin\delta. \quad (5.12)$$

Equation (5.12) may be written in the form given as

$$\boxed{E^* = E' + iE''} \quad (5.13)$$

where E' is called the (tensile) *storage modulus* given as

$$E' = \left(\frac{\sigma^o}{\varepsilon^o} \right) \cos\delta \quad (5.14)$$

and E'' is the (tensile) *loss modulus*:

$$E'' = \left(\frac{\sigma^o}{\varepsilon^o} \right) \sin \delta. \quad (5.15)$$

The ratio of loss and storage moduli defines another useful parameter in dynamic-mechanical analysis called $\tan \delta$ where

$$\boxed{\tan \delta = \frac{\sin \delta}{\cos \delta} = \frac{E''}{E'}}. \quad (5.16)$$

As in static testing (see Section 4.4.2) where the tensile modulus is the inverse of the compliance, the dynamic tensile modulus is inversely related to the dynamic tensile compliance, D^* , as

$$D^* = \frac{1}{E^*} = \frac{\varepsilon^*}{\sigma^*} = \frac{\varepsilon^o \exp(i\omega t)}{\sigma^o \exp[i(\omega t + \delta)]} = \left(\frac{\varepsilon^o}{\sigma^o} \right) \exp(-i\delta). \quad (5.17)$$

Substitution of Euler's identity in the form of $\exp(-i\delta) = \cos \delta - i \sin \delta$ into eq. (5.17) gives

$$D^* = \left(\frac{\varepsilon^o}{\sigma^o} \right) \cos \delta - i \left(\frac{\varepsilon^o}{\sigma^o} \right) \sin \delta. \quad (5.18)$$

Equation (5.18) may be written in the form

$$D^* = D' = -iD'' \quad (5.19)$$

where D' is called the *storage compliance*,

$$D' = \left(\frac{\varepsilon^o}{\sigma^o} \right) \cos \delta, \quad (5.20)$$

and D'' is the (tensile) *loss compliance*,

$$D'' = \left(\frac{\varepsilon^o}{\sigma^o} \right) \sin \delta. \quad (5.21)$$

The negative sign of the second term (i.e., $-iD''$) in the RHS of eq. (5.19) contrasts with the corresponding positive term (i.e., $+iE''$) in eq. (5.13). As in the case of dynamic modulus (eq. (5.16)), $\tan \delta$ is related to the components of the complex dynamic compliance as

$$\tan \delta = \frac{D''}{D'} . \quad (5.22)$$

It is possible to obtain values of dynamic storage and loss moduli from corresponding values of compliance, and vice versa, by manipulation of their complex conjugates. The complex conjugate of the dynamic modulus (eq. (5.13)) is

$$\overline{E^*} = E' - iE'' . \quad (5.23)$$

The *magnitude* of the dynamic modulus, $|E^*|$, is obtained from its complex conjugate as

$$E^* \times \overline{E^*} = |E^*|^2 = (E')^2 + (E'')^2 . \quad (5.24)$$

Then (from eqs. (5.17), (5.23), and (5.24)), we can write

$$D^* = \frac{1}{E^*} = \frac{\overline{E^*}}{(E')^2 + (E'')^2} = \frac{E'}{(E')^2 + (E'')^2} - i \left[\frac{E''}{(E')^2 + (E'')^2} \right] . \quad (5.25)$$

Comparison of the form of eq. (5.25) with the expression for D^* (eq. (5.19)) gives the interrelationships between the components of dynamic modulus and dynamic compliance:

$$D' = \frac{E'}{(E')^2 + (E'')^2} \quad (5.26)$$

and

$$D'' = \frac{E''}{(E')^2 + (E'')^2} . \quad (5.27)$$

Similar relationships may be written for E' and E'' as functions of D' and D'' .

Work in Dynamic Deformation. As is the case for other forms of mechanical deformation, work is expended during dynamic-mechanical testing. The amount of work, or power, consumed depends upon the viscoelastic properties of the polymer. The work *per unit of sample volume*, W , may be expressed in terms of stress and strain as

$$W = \int \left(\frac{f}{V} \right) d\ell = \int \left(\frac{f}{A} \right) \frac{d\ell}{\ell} = \int \sigma d\varepsilon \quad (5.28)$$

where f is the force, $d\ell$ is the differential extension of the sample, and V is the sample volume. Per cycle (i.e., 2π radians) of oscillation, the *dynamic* work (now given per unit volume and cycle) is then obtained as

$$W = \int_0^{2\pi} \sigma^* d\varepsilon^*. \quad (5.29)$$

Substitution of the appropriate expressions for σ^* (from eq. (5.2)) and $d\varepsilon^*$ (from eq. (5.5)) and integration of eq. (5.29) gives the work per cycle per unit volume for dynamic oscillation of a viscoelastic solid (see Problem 5.2) as

$$W = \pi \sigma^\circ \varepsilon^\circ \sin \delta. \quad (5.30)$$

Rearrangement of eq. (5.15) gives

$$\sin \delta = \left(\frac{\varepsilon^\circ}{\sigma^\circ} \right) E''$$

which can be substituted into eq. (5.30) to obtain

$$W = \pi (\varepsilon^\circ)^2 E''. \quad (5.31)$$

From a consideration of the $\sin \delta$ contribution to W in eq. (5.30), it is obvious that the work of oscillation for an ideal elastic solid (i.e., $\delta = 0$ and $\sin \delta = 0$) is zero, while the maximum work is expended during deformation of an ideal viscous material (i.e., $\delta = \pi/2$, $\sin \delta = 1$, and $W = \pi \sigma^\circ \varepsilon^\circ$). The *power* consumed per unit volume is then obtained by multiplying the work per cycle (per unit volume) given by eq. (5.30) or (5.31) by the number of cycles per unit time (i.e., $f = \omega / 2\pi$) as

$$P = \left(\frac{\omega}{2} \right) \sigma^\circ \varepsilon^\circ \sin \delta = \left(\frac{\omega}{2} \right) (\varepsilon^\circ)^2 E''. \quad (5.32)$$

Experimental Techniques. The usual way to report the viscoelastic response of a polymer is by means of a semilog plot of storage modulus and loss modulus (or $\tan \delta$) as a function of temperature at one or more frequencies. The temperature range may be very broad—often extending from liquid-nitrogen temperatures (ca. -150°C) to temperatures in the range of T_g that can be 200°C or more. The dynamic storage modulus behaves much like the tensile (or shear) modulus as a function of temperature (see Figure 4-19). Maxima in loss modulus, or $\tan \delta$, occur both at T_g and at low temperatures, where small-scale molecular motions can occur (i.e., secondary relaxations). In the case of semicrystalline polymers, an additional peak in $\tan \delta$ corresponding to T_m will occur above T_g . Traditionally, the highest-temperature peak is designated the α relaxation (i.e., the glass transition in amorphous polymers).

phous polymers and the crystalline-melting transition in semicrystalline polymers), the next highest is the β relaxation, then the γ relaxation, and so on.

A number of different instruments have been used to obtain dynamic-mechanical data. The earliest designs used a *free-vibration* approach (torsion pendulum and torsional braid) in which a polymer sample in the form of a bar or cylinder is set to oscillate and the damping of the oscillation is recorded as a function of time at constant temperature. More recent instrumentation employs *forced oscillation* whereby a sinusoidal strain (tensile, flexure, compression, shear, or torsional) is applied and the stress response is recorded as a function of temperature at different frequencies. These techniques are described in the following sections.

Free-Vibration Methods. The simplest and earliest dynamic-mechanical technique, the *torsion pendulum*, is a free-vibration technique [1]. In this experiment, a polymer film is rigidly clamped at one end, while the other end is attached to an inertia disk that is free to oscillate. Once the disk is set in oscillation, the viscous response of the polymer sample causes the amplitude of the oscillation to decay, as illustrated in Figure 5-2. The time required for one complete oscillation is called the *period* of oscillation (P).

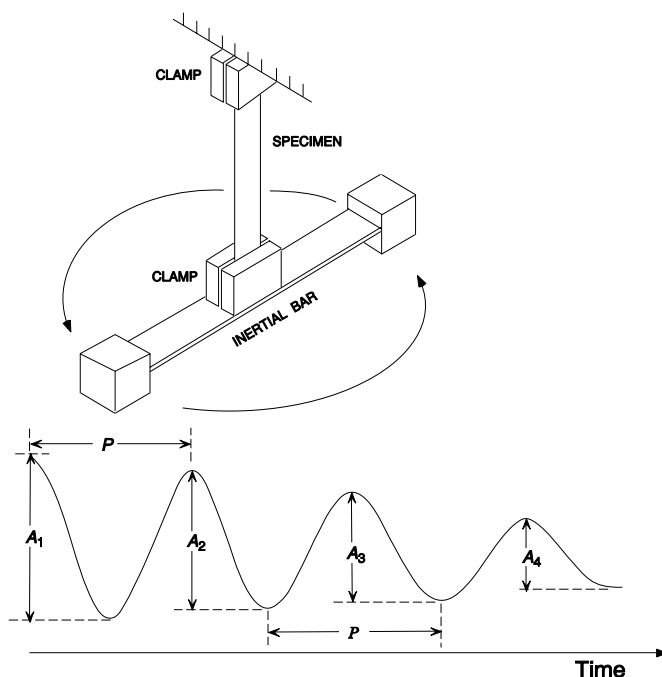


Figure 5-2 Torsion-pendulum apparatus (top) and a plot of amplitude of oscillation (bottom). Adapted from L. Nielsen, *Dynamic Mechanical Properties of High Polymers*. SPE Journal, 1960.16: p. 525–532.

The value of $\tan \delta$ can be determined from the ratio of amplitudes (A) of any two consecutive peaks as

$$\Delta = \pi \tan \delta = \ln \frac{A_1}{A_2}. \quad (5.33)$$

where δ is called the *log decrement*. Frequencies of disk oscillation may range from 0.01 to 50 Hz as determined by sample characteristics. Usually, frequency is approximately 1 Hz and will vary slightly with temperature over the course of the experiment.

Since the mode of deformation is actually torsion, it is usual to represent the response in terms of dynamic *shear moduli*, G' and G'' (where $G^* = G' + iG''$). The shear *storage modulus*, G' , is obtained from the sample geometry (F_s), moment of inertia (I), and period of oscillation (P) as

$$G' = F_s I \left(\frac{1}{P^2} \right). \quad (5.34)$$

The relationships from which the geometry factor may be calculated depend upon whether the sample is cylindrical or rectangular [2]. For a rectangular sample, the geometry parameter is given as

$$F_s = \frac{64\pi^2 L}{u W t^3} \quad (5.35)$$

where L is the sample length, W is width, t is thickness, and u is a shape factor that depends upon the (aspect) ratio of the samples (W/t). Once G' and $\log \Delta$ have been measured, the shear loss modulus, G'' can be calculated as

$$G'' = G' \tan \delta = \frac{G' \Delta}{\pi}. \quad (5.36)$$

As an example of dynamic-mechanical data, values of the storage modulus and log decrement obtained by early torsion-pendulum measurements [1] of poly(methyl methacrylate) (PMMA) are plotted against temperature in Figure 5-3. The data indicate an α relaxation corresponding to T_g (i.e., maximum in $\log \Delta$ and sharp decrease in the value of G') near 130°C and a (β) secondary-relaxation peak (see Section 4.1.3) near 40°C. A small drop in G' accompanies the broad maximum in $\log \Delta$ at the β relaxation. The β relaxation was attributed in this study to the motion of the large ($-COOCH_3$) pendant group of PMMA whose structure is as follows:

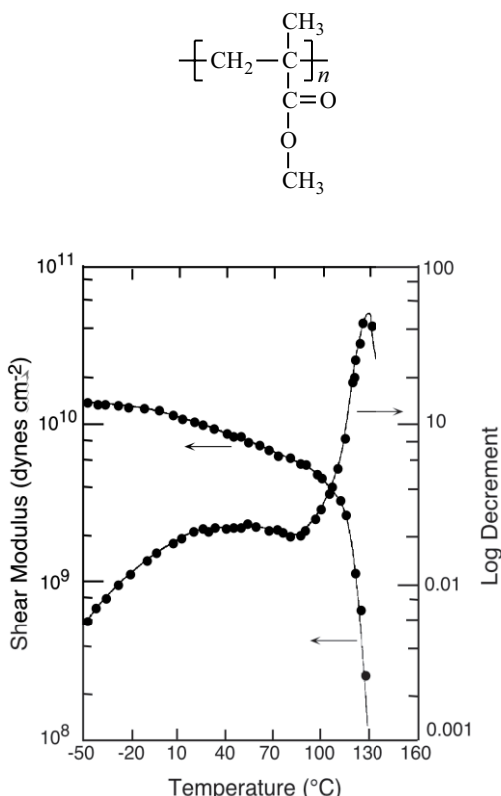


Figure 5-3 Values of the shear modulus (G) and log decrement (Δ) of poly(methyl methacrylate) plotted as a function of temperature. Data were obtained by torsion-pendulum measurements [1].

The torsion pendulum is still actively used today and is available commercially as a fully automated instrument. A schematic diagram of a modern torsion-pendulum apparatus is shown in Figure 5-4. Temperature can be controlled to within $\pm 0.05^\circ\text{C}$ isothermally from 25° to 400°C or may be ramped up or down at rates of 0.1°C h^{-1} to 5°C min^{-1} from -180° to 400°C . The frequency and damping are optically tracked for data acquisition. As shown in Figure 5-4, a light beam passes through a pair of polarizers housed in the optical cage. The upper polarizer oscillates with the specimen, and the intensity of light measured by means of a non-drag optical transducer is a linear function of the angular displacement of the pendulum.

An important variation of the torsion-pendulum technique is called *torsional-braid analysis* (TBA) [3]. Instrumentation is the same as used for torsion-pendulum analysis of films, rods, or bars; however, the TBA sample is *supported* on a braid, typically made from glass fibers. The braid is coated with a dilute solution of the

sample and dried in a vacuum to remove all solvent. Although the quantitative values of dynamic moduli of this composite geometry are *not* the same as the unsupported polymer, the *qualitative* dependence of $\tan\delta$ on temperature is a good representation of the actual polymer response. The advantage of this technique is that the support provided by the braid enables the dynamic-mechanical characterization of low-molecular-weight and *liquid* samples as well as high-molecular-weight polymer samples near and above T_g , where softening would preclude the use of unsupported-sample techniques. For example, the cure of an epoxy resin can be followed by recording the increase in G' with time at a fixed temperature.

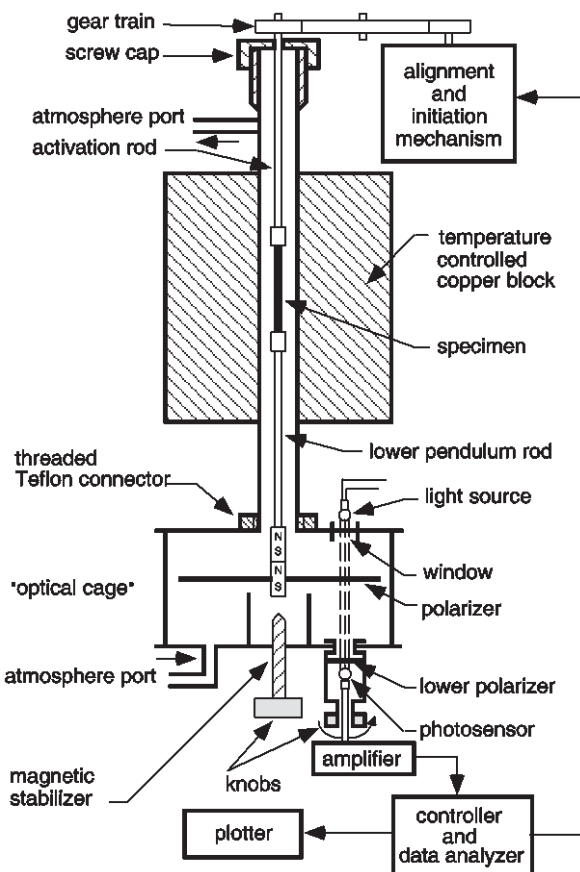


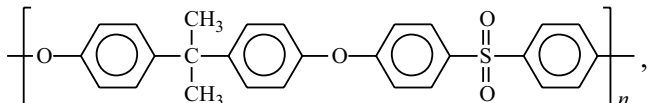
Figure 5-4 Schematic diagram of a commercial torsion-pendulum apparatus. Courtesy of J. K. Gillham.

As an illustration of TBA data, the loss modulus of PMMA samples [4] with different tacticity is plotted against temperature in Figure 5-5. Results indicate that

the lowest T_g (determined as the temperature at the maximum of the high-temperature α peak) is observed for isotactic PMMA, *i*-PMMA, ($T_g = 334$ K), while the T_{gS} of atactic PMMA (*a*-PMMA) and syndiotactic PMMA (*s*-PMMA) are higher and nearly equal (i.e., 384 K for *a*-PMMA and 399 K for *s*-PMMA). These values compare favorably with T_{gS} determined by calorimetric measurements of *i*-PMMA (318 K), *a*-PMMA (378 K), and *s*-PMMA (388 K) [5]. In contrast, the temperatures corresponding to the β peaks are nearly invariant, but the magnitude of the β peak decreases with increasing isotactic content. The decrease in the intensity of the β peak for the isotactic form of PMMA is believed to be due to the immobilization of the ester substituent groups in the (5/1) helical conformation* of this crystalline isomer.

Forced-Vibration Methods. Today, the most frequently used commercial instruments utilize a *forced-* (rather than free-) vibration method by which a dynamic tensile, compressive, torsional, or flexural strain is applied to the sample, which is cut or molded in the form of a thin film or bar. One important advantage of the forced-vibration mode is that frequency can be controlled precisely over a wider range (0.001 to 100 rad s⁻¹) than is possible for free-vibration methods. As discussed next, comparison of dynamic-mechanical spectra obtained at several frequencies provides useful additional information on the viscoelastic properties of the polymer. Section 5.1.4 outlines the principles of dielectric spectroscopy, which provides viscoelastic information over a much wider range of frequencies (up to 10¹⁰ Hz).

A representative dynamic-mechanical spectrum of an engineering thermoplastic, polysulfone, whose chemical structure is



is shown in Figure 5-6. In this example, the dynamic-mechanical data were obtained by forced-vibration instrumentation at 10 rad s⁻¹ (ca. 1.6 Hz) in the tensile mode [6]. In addition to the glass transition (α peak), which occurs near 481 K (188°C), there is a major secondary-relaxation process (the γ peak) showing a broad maximum located near 166 K (-107°C). It is believed that this low-temperature transition reflects short-range mobility of the main chain including flips of phenylene rings and possibly coupled rotations of methyl groups. There is also a suggestion of a small, very broad transition (β peak) at intermediate temperatures near 340 K. This peak appears to be sensitive to the thermal history of the sample and is believed to be asso-

* The first number identifying the conformational form of a helix indicates the number of repeating units participating in a given number of turns of the helix. In the case of a 5/1 (or 5₁) helix, five repeating units form one complete turn of the helix.

ciated with limited segmental motions appearing as a precursor to the longer-range motions occurring at the glass transition.

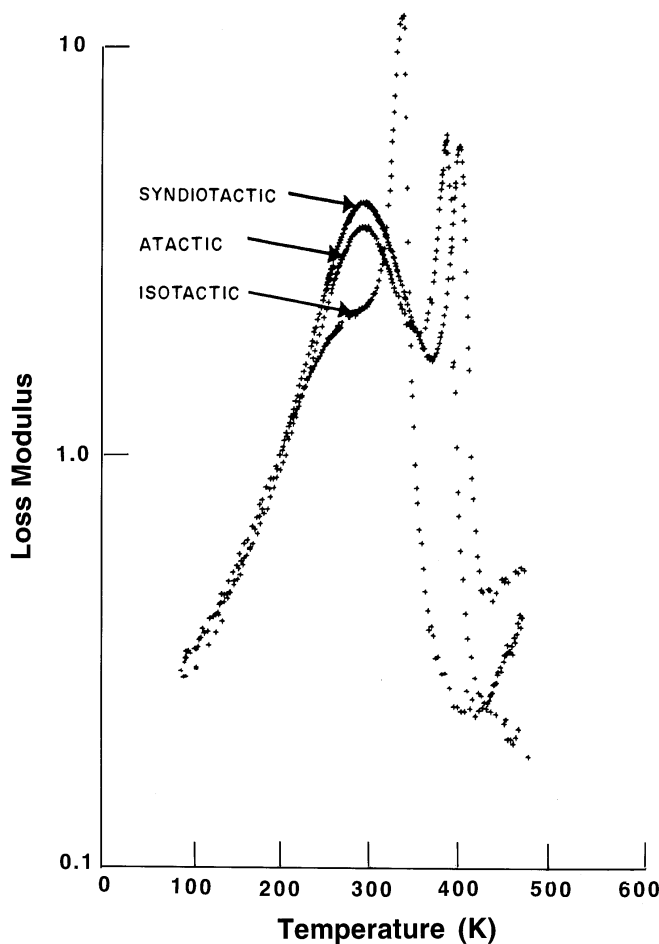


Figure 5-5 Loss-modulus data for PMMA samples with different tacticities as obtained by torsion-braid analysis at a heating rate of $2^{\circ}\text{C min}^{-1}$. From J. K. Gillham, S. J. Stadnicki, and Y. Hazony, Journal of Applied Polymer Science, 1977, 21: p. 401. Copyright © 1977 John Wiley & Sons. Reprinted by permission of John Wiley & Sons, Inc.

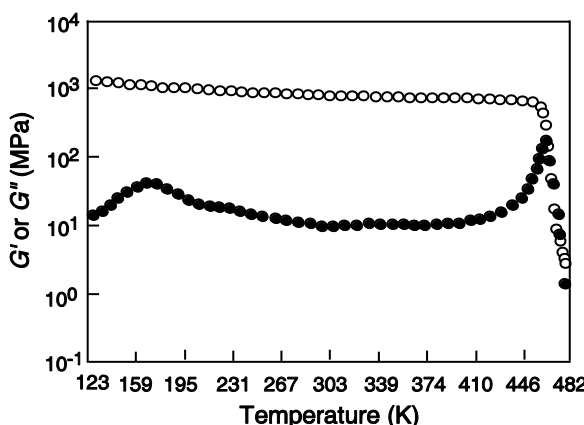


Figure 5-6 Dynamic-mechanical spectrum of polysulfone obtained in forced torsion at 10 rad s^{-1} ($\sim 1.6 \text{ Hz}$) [6]. Data points indicate (○) shear storage-modulus (G') and (●) shear loss modulus (G''). A low-temperature, secondary-relaxation (γ) peak with a broad maximum near 166 K (-107°C) appears in the loss-modulus plot. The glass transition (i.e., α peak) occurs at 481 K (188°C).

Activation Energies. Energies required for main-chain and side-group motions can be obtained by determining the effect of frequency on the maximum temperatures of the loss, or $\tan \delta$, peaks. The ability to vary oscillation frequency makes forced-vibration techniques the choice for these studies. The temperature at the peak maxima, T_{\max} , increases with increasing frequency, and the activation energy, E_a , of the relaxational process may be determined from the slope of a semilog plot of frequency (f or ω) versus reciprocal peak temperature ($1/T_{\max}$) as

$$\ln f = -\left(\frac{E_a}{R}\right)\frac{1}{T_{\max}} + \ln f_0 \quad (5.37)$$

where f_0 is a constant obtained from the intercept. Typically, activation energies for low-temperature (i.e., secondary) relaxations are low (ca. 10 to 20 kcal mol⁻¹). In the example of the dynamic-mechanical spectra of poly(methyl methacrylate) shown in Figure 5-3, the activation energy of the β peak was reported to be approximately 17 kcal mol⁻¹. The activation energy for the γ relaxation of polysulfone (Figure 5-6) was reported to be 10.7 kcal mol⁻¹, in agreement with predictions of semiempirical molecular-orbital calculations of the energy barriers to rotation for the phenylene rings in the backbone of the polysulfone chain [6]. Corresponding activation energies for the glass transition, reflecting longer-range cooperative motions, are about an order of magnitude greater than those for secondary relaxations. For example,

the activation energy of the α (glass) relaxation of polysulfone is approximately 220 kcal mol⁻¹ [6]. High activation energies mean that the temperature location of the α (glass) relaxation is relatively insensitive to a change in frequency compared to secondary-relaxation processes. Principal relaxations and activation energies for a number of different polymers are given in several sources [7, 8].

5.1.2 Mechanical Models of Viscoelastic Behavior

An insight into the nature of the viscoelastic properties of polymers can be obtained by analyzing the stress or strain response of mechanical models using an ideal spring as the Hookean element and a dashpot as the viscous element. A dashpot may be viewed as a shock absorber consisting of a piston in a cylinder filled with a Newtonian fluid of viscosity η . The elemental models are a series combination of a spring and dashpot, the *Maxwell* element, and a parallel combination of a spring and dashpot, the *Voigt* element, as illustrated in Figure 5-7. In the following sections, relationships for the transient and dynamic responses of Maxwell and Voigt models are developed.

Maxwell Element. In the case of a series combination of a spring and dashpot, the total strain (or strain rate) is a summation of the individual strains (or strain rates) of the spring and dashpot. From Hooke's law ($\sigma = E\varepsilon$), the strain *rate* of an ideal elastic spring can be written as

$$\frac{d\varepsilon}{dt} = \left(\frac{1}{E} \right) \frac{d\sigma}{dt} \quad (5.38)$$

while the strain rate for the dashpot is obtained by rearranging Newton's law of viscosity (eq. (5.4)) as

$$\frac{d\varepsilon}{dt} = \frac{\sigma}{\eta}. \quad (5.39)$$

Therefore, the basic equation for strain rate in the Maxwell model is the summation of the strain rates for the spring and dashpot (eqs. (5.38) and (5.39)) as

$$\boxed{\frac{d\varepsilon}{dt} = \left(\frac{1}{E} \right) \frac{d\sigma}{dt} + \frac{\sigma}{\eta}}. \quad (5.40)$$

This differential equation can be solved for creep, stress relaxation, and dynamic response by applying the appropriate stress or strain function.

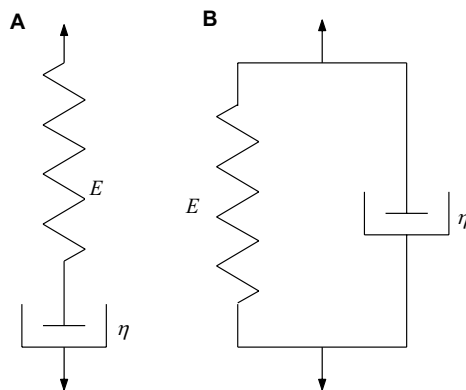


Figure 5-7 Maxwell (**A**) and Voigt (**B**) elements.

In a *creep* experiment (see Section 4.4.2), a *constant* stress, σ_0 , is applied instantaneously. Equation (5.40) then reduces to

$$\frac{d\varepsilon}{dt} = \frac{\sigma_0}{\eta}. \quad (5.41)$$

Rearrangement and integration of eq. (5.41) give

$$\varepsilon(t) = \left(\frac{\sigma_0}{\eta} \right) t + \varepsilon_0 \quad (5.42)$$

where ε_0 represents the *instantaneous* (i.e., $t = 0$) strain response of the spring element. The creep compliance function, $D(t)$, is then obtained as

$$D(t) = \frac{\varepsilon(t)}{\sigma_0} = \frac{t}{\eta} + \frac{\varepsilon_0}{\sigma_0} = \frac{t}{\eta} + D \quad (5.43)$$

where $D (= \varepsilon_0 / \sigma_0)$ is the instantaneous compliance (of the spring). An alternative form of eq. (5.43) may be obtained by defining a *relaxation time*, τ , as

$$\tau = \frac{\eta}{E} = \eta D.$$

(5.44)

Equation (5.43) can then be represented in normalized form as

$$\frac{D(t)}{D} = \frac{t}{\tau} + 1. \quad (5.45)$$

In a *stress-relaxation* experiment (see Section 4.4.2), the strain (ε_0) is constant and, therefore, the strain rate is zero. Equation (5.40) then reduces to the first-order ordinary differential equation

$$\left(\frac{1}{E}\right)\frac{d\sigma}{dt} + \frac{\sigma}{\eta} = 0. \quad (5.46)$$

Rearrangement of eq. (5.46) and introduction of τ give

$$\frac{d\sigma}{\sigma} = -\left(\frac{1}{\tau}\right)dt. \quad (5.47)$$

Integration yields the stress response as

$$\sigma = \sigma_0 \exp\left(\frac{-t}{\tau}\right) \quad (5.48)$$

where σ_0 is the instantaneous stress response of the spring. The stress relaxation modulus, $E_r(t)$, is then obtained as

$$E_r(t) = \frac{\sigma}{\varepsilon_0} = \left(\frac{\sigma_0}{\varepsilon_0}\right) \exp\left(\frac{-t}{\tau}\right) = E \exp\left(\frac{-t}{\tau}\right) \quad (5.49)$$

where $E (= \sigma_0/\varepsilon_0)$ is the (Young's) modulus of the spring element.

To obtain an expression for the *dynamic-mechanical* response (i.e., complex compliance or modulus), the expression for complex stress, $\sigma = \sigma^0 \exp(i\omega t)$, is substituted into the Maxwell equation (eq. (5.40)) to give

$$\frac{d\varepsilon(t)}{dt} = \left(\frac{\sigma^0}{E}\right) i\omega \exp(i\omega t) + \left(\frac{\sigma^0}{\eta}\right) \exp(i\omega t). \quad (5.50)$$

Integration from time t_1 to t_2 gives

$$\varepsilon(t_2) - \varepsilon(t_1) = \left(\frac{\sigma^0}{E}\right) [\exp(i\omega t_2) - \exp(i\omega t_1)] + \left(\frac{\sigma^0}{\eta i\omega}\right) [\exp(i\omega t_2) - \exp(i\omega t_1)]. \quad (5.51)$$

Since the corresponding stress increment can be written as

$$\sigma(t_2) - \sigma(t_1) = \sigma^0 [\exp(i\omega t_2) - \exp(i\omega t_1)], \quad (5.52)$$

division of both sides of eq. (5.51) by this expression, and making use of τ , gives the complex compliance as

$$D^* = D - i \left(\frac{D}{\omega \tau} \right). \quad (5.53)$$

Therefore, the storage compliance obtained from the Maxwell model is simply the compliance of the spring

$$D' = D, \quad (5.54)$$

which is independent of time or frequency, while the loss compliance is

$$D'' = \frac{D}{\omega \tau}. \quad (5.55)$$

The corresponding expression for complex modulus, E^* , is obtained by recalling that E^* is the reciprocal of D^* and utilizing the complex conjugate of D^* as

$$E^* = \frac{1}{D^*} = \frac{1}{D - i \frac{D}{\omega \tau}} \times \frac{D + i \frac{D}{\omega \tau}}{D + i \frac{D}{\omega \tau}}. \quad (5.56)$$

Performing the multiplication, rearranging, and using the inverse relation $E = 1/D$ gives

$$E^* = E' + iE'' = \frac{E(\omega \tau)^2}{1 + (\omega \tau)^2} + i \left[\frac{E\omega \tau}{1 + (\omega \tau)^2} \right] \quad (5.57)$$

where

$$E' = \frac{E(\omega \tau)^2}{1 + (\omega \tau)^2} \quad (5.58)$$

and

$$E'' = \frac{E\omega \tau}{1 + (\omega \tau)^2}. \quad (5.59)$$

It follows from eqs. (5.58) and (5.59) that $\tan \delta$ for a Maxwell model is simply

$$\tan \delta = \frac{E''}{E'} = \frac{1}{\omega \tau}. \quad (5.60)$$

Voigt Element. For a parallel combination of a spring and dashpot, the Voigt model shown in Figure 5-7B, the strain on each element must be equal while the stress is additive. The fundamental relation for the Voigt model is, therefore,

$$\boxed{\sigma = E\varepsilon + \eta \frac{d\varepsilon}{dt}}. \quad (5.61)$$

Making use of the relaxation time (eq. (5.44)), the Voigt equation for creep deformation becomes a linear differential equation,

$$\frac{\sigma_0}{\eta} = \frac{\varepsilon(t)}{\tau} + \frac{d\varepsilon(t)}{dt} \quad (5.62)$$

which can be solved by using the integrating factor $\exp(t/\tau)$. Solving for $\varepsilon(t)$ gives the compliance function as

$$D(t) = D \left[1 - \exp\left(\frac{-t}{\tau}\right) \right] \quad (5.63)$$

where $D = 1/E$. In contrast to the Maxwell model, the Voigt equation cannot be solved in any meaningful way for stress relaxation because the dashpot element cannot be deformed instantaneously.

The response of a Voigt model to dynamic strain gives the relationships for the storage and loss compliance as

$$D' = \frac{D}{1 + (\omega\tau)^2} \quad (5.64)$$

and

$$D'' = \frac{D\omega\tau}{1 + (\omega\tau)^2}. \quad (5.65)$$

The forms of these relationships for compliance are the same as those for dynamic moduli (eqs. (5.58) and (5.59)) given by the Maxwell model.

Comparison of Simple Models. The two-element models approximate some of the viscoelastic properties of real polymers. Results are summarized in Table 5-1. In general, modulus is modeled best by the Maxwell element, while compliance is better represented by the Voigt element. The most significant limitation of these two models is that they employ only a single relaxation time (eq. (5.44)). This results in the prediction of only a *single transition* in modulus or compliance, whereas high-molecular-weight polymers exhibit both a glass-to-rubber and rubber-to-liquid tran-

sition. As would be expected, improvement is achieved by adding more elements, as discussed in the following section.

Table 5-1 Predictions of Viscoelastic Properties by the Maxwell and Voigt Models

Experiment	Maxwell Model	Voigt Model
Creep	$\frac{D(t)}{D} = 1 + \frac{t}{\tau}$	$\frac{D(t)}{D} = 1 - \exp\left(-\frac{t}{\tau}\right)$
Stress relaxation	$\frac{E(t)}{E} = \exp\left(-\frac{t}{\tau}\right)$	$\frac{E(t)}{E} = 1$
Dynamic mechanical	$\frac{D'}{D} = 1$	$\frac{D'}{D} = \frac{1}{1 + (\omega t)^2}$
	$\frac{D''}{D} = \frac{1}{\omega \tau}$	$\frac{D''}{D} = \frac{\omega \tau}{1 + (\omega \tau)^2}$
	$\frac{E'}{E} = \frac{(\omega \tau)^2}{1 + (\omega \tau)^2}$	$E' = E$
	$\frac{E''}{E} = \frac{\omega \tau}{1 + (\omega \tau)^2}$	$E'' = \omega \eta$

Multi-element Models. A multi-element model, particularly suited for modulus, is called the *Maxwell–Wiechert model*, which is a parallel combination of multiple Maxwell elements. In this model, the strains on each Maxwell element are equal and the stresses experienced by each Maxwell element are additive, as they are in the case of the single spring and dashpot in the simple Voigt model. For the two-element Maxwell–Wiechert model illustrated in Figure 5-8, the stress-relaxation modulus is given as

$$E(t) = E_1 \exp\left(-\frac{t}{\tau_1}\right) + E_2 \exp\left(-\frac{t}{\tau_2}\right) \quad (5.66)$$

where $\tau_1 = \eta_1 / E_1$ and $\tau_2 = \eta_2 / E_2$. By appropriate selection of values for E_i and τ_i , a reasonable representation of the glass and rubber plateau regions of the stress-relaxation modulus is obtained, as illustrated in Figure 5-9.

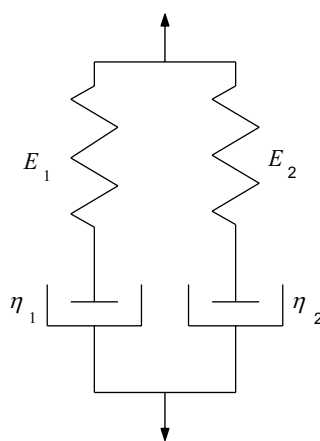


Figure 5-8 Representation of a two-element Maxwell–Wiechert model.

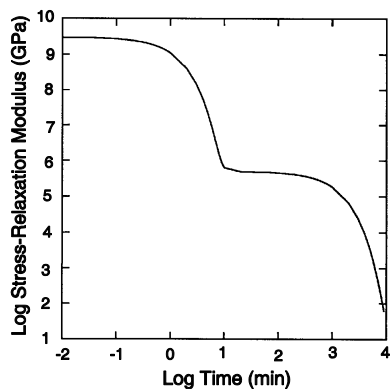


Figure 5-9 Prediction of stress-relaxation modulus, $E(t)$, as a function of dimensionless time (t/τ) for the two-element Maxwell–Wiechert model illustrated in Figure 5-8. Values for model parameters (eq. (5.66)) are $E_1 = 3 \times 10^9$ Pa, $E_2 = 5 \times 10^5$ Pa, $\tau_1 = 1$ min, and $\tau_2 = 10^3$ min.

Further improvement in terms of realistic slopes in the transition regions is obtained by adding additional Maxwell elements in the model and, therefore, providing a distribution of relaxation times as would be expected for a high-molecular-weight polymer with a broad distribution of molecular weights. In general, the stress-relaxation modulus of a Maxwell–Wiechert model consisting of N Maxwell elements can be written as the summation

$$E(t) = \sum_{i=0}^N E_i \exp\left(\frac{-t}{\tau_i}\right). \quad (5.67)$$

Corresponding equations can be written for dynamic moduli, as shown in Table 5-2.

Table 5-2 Predictions of Viscoelastic Properties by Two Multi-element Models, Maxwell–Wiechert and Voigt–Kelvin

Experiment	Maxwell–Wiechert Model	Voigt–Kelvin Model
Creep		$D(t) = \sum_{i=1}^N D_i \left[1 - \exp\left(\frac{-t}{\tau_i}\right) \right]$
Stress relaxation	$E(t) = \sum_{i=1}^N E_i \exp\left(\frac{-t}{\tau_i}\right)$	
Dynamic mechanical	$E' = \sum_{i=1}^N \frac{E_i (\omega \tau_i)^2}{1 + (\omega \tau_i)^2}$	$D' = \sum_{i=1}^N \frac{D_i}{1 + (\omega \tau_i)^2}$
	$E'' = \sum_{i=1}^N \frac{E_i \omega \tau_i}{1 + (\omega \tau_i)^2}$	$D'' = \sum_{i=1}^N \frac{D_i \omega \tau_i}{1 + (\omega \tau_i)^2}$

An alternative approach for a multi-element model is a *Voigt–Kelvin model*, which consists of a *series* arrangement of Voigt elements. A two-element Voigt–Kelvin model is illustrated in Figure 5-10. For N elements, the creep compliance can be written as a summation:

$$D(t) = \sum_{i=0}^N D_i \left[1 - \exp\left(\frac{-t}{\tau_i}\right) \right]. \quad (5.68)$$

Corresponding equations can be written for dynamic compliance as given in Table 5-2.

Relaxation and Retardation Spectra. In the limit of an infinite number of Maxwell elements in a Maxwell–Wiechert model, the summation given in eq. (5.67) may be replaced by an integral:

$$E(t) = \int_0^\infty E(\tau) \exp\left(\frac{-t}{\tau}\right) d\tau. \quad (5.69)$$

In this equation, $E(\tau)$ is a continuous function of the relaxation times. An alternative expression is given as

$$H(\tau) = \tau E(\tau) \quad (5.70)$$

where $H(\tau)$ is called the *relaxation-time distribution function*. Substitution of this relation into the integral and using $\ln \tau$ in place of τ gives

$$E(t) = \int_{\ln \tau = -\infty}^{\ln \tau = +\infty} H(\tau) \exp\left(\frac{-t}{\tau}\right) d\ln \tau. \quad (5.71)$$

Corresponding expressions can be written for the dynamic moduli.

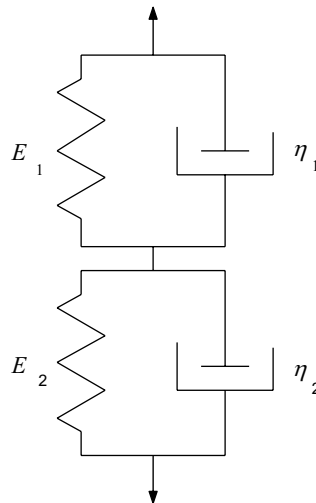


Figure 5-10 Representation of a two-element Voigt–Kelvin model.

An expression for compliance is obtained by considering an infinite number of Voigt elements in series (Voigt–Kelvin model)

$$D(t) = \int_{\ln \tau = -\infty}^{\ln \tau = +\infty} L(\tau) \left[1 - \exp\left(\frac{-t}{\tau}\right) \right] d\ln \tau, \quad (5.72)$$

where $L(\tau)$ is called the *retardation spectrum function*. Corresponding expressions can be written for the dynamic moduli.

Relaxation and retardation spectra characterize the viscoelastic properties of a polymer at a particular temperature. They can be calculated from one set of experimental data and then be used to predict the viscoelastic response under different experimental conditions. For example, the relaxation-time spectrum can be calculated from the temperature dependence of the dynamic loss modulus and then be used to calculate the temperature dependence of the stress-relaxation modulus. Such interre-

lationships minimize experimental work and provide a basis to test the consistency of experimental data.

5.1.3 Viscoelastic Properties of Polymer Solutions and Melts

Concentrated polymer solutions and melts also exhibit viscoelastic response. It is convenient to characterize this response in terms of a complex viscosity, η^* . This is defined by applying Newton's law of viscosity (eq. (5.4)) to the case of a dynamically applied shear strain, γ^* ($= \gamma_0 e^{i\omega t}$). The corresponding dynamic shear stress, τ^* , is then written as

$$\tau^* = \eta^* \frac{d\gamma^*}{dt} = i\omega \eta^* \gamma^*. \quad (5.73)$$

The complex viscosity can be written in a form analogous to dynamic compliance,

$$\boxed{\eta^* = \eta' - i\eta''}, \quad (5.74)$$

where η' is called the *dynamic viscosity* and is obtained from the values of the shear loss modulus (G'') and angular frequency, ω , as^{*}

$$\eta' = \frac{G''}{\omega}. \quad (5.75)$$

The imaginary component of the viscosity, η'' , is obtained from the shear storage modulus, G' , as

$$\eta'' = \frac{G'}{\omega}. \quad (5.76)$$

The *Cox–Merz rule* provides an approximate relationship between the *steady-shear viscosity* in the limit of zero shear rate, η_0 (see Section 11.2.1), and the magnitude of the complex viscosity as

$$\eta_0 = |\eta^*| = \left[(\eta')^2 + (\eta'')^2 \right]^{1/2}. \quad (5.77)$$

^{*} Equations (5.75) and (5.76) follow from eq. (5.73) as

$$G^* = G' + iG'' = \frac{\tau^*}{\gamma^*} = i\omega \eta^* = i\omega(\eta' - i\eta'') = \omega(\eta'' + i\eta').$$

Experimental Techniques. Commercial instrumentation to determine the stress response of polymeric solutions and melts to small (i.e., linear viscoelastic) static or dynamic shear strains is based on simple-shear geometries such as cone-and-plate, concentric (Couette) cylinder, and rotating parallel plates. The rate of applied strain for these instruments is low (10^{-4} to 10^3 s^{-1}). Two of these rheometers, cone-and-plate and concentric cylinder, are described in detail in Section 11.4 in relation to their importance in determining the *apparent viscosity* of polymer melts and concentrated solutions as a function of frequency or shear strain rate at low shear rates. Basic principles of rheometry are described in a variety of sources [9, 10].

The apparent viscosity, as defined by Newton's law of viscosity (eq. (5.4)), is obtained from steady-shear measurements as

$$\eta = \frac{\tau}{\dot{\gamma}}. \quad (5.78)$$

Values of complex viscosity or, equivalently, the real and imaginary components of the shear moduli, G' and G'' , are obtained by applying an *oscillatory* rather than steady shear to the cone in a cone-and-plate rheometer or to the cylinder in the case of a Couette rheometer.

Alternatively, the dynamic properties (i.e., G' and G'') of polymer solutions and melts can be obtained directly by using *steady-shear flow* in a rheometer employing an eccentric rotating-disk (ERD) geometry that is illustrated in Figure 5-11. In this rheometer design, the plates are parallel, but the axes perpendicular to the plates are offset by a preset distance, a . This offset results in a flow parallel to the plates that is periodic in time (i.e., dynamic flow), although the top plate is driven at a constant angular frequency, ω . The shear rate is given as

$$\dot{\gamma} = \left(\frac{a}{h} \right) \omega. \quad (5.79)$$

The dynamic moduli are determined from geometric parameters—axes offset (a), plate radius (R), and plate separation (h)—and forces measured in the orthogonal directions (F_x and F_y) as follows:

$$G' = \frac{F_y h}{a \pi R^2} \quad (5.80)$$

and

$$G'' = \frac{F_x h}{a \pi R^2}. \quad (5.81)$$

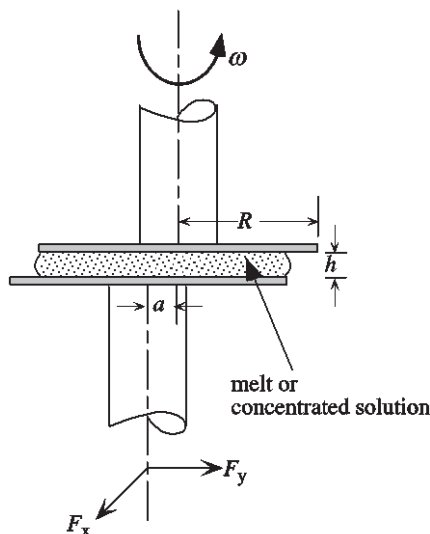


Figure 5-11 Eccentric rotating-disk (ERD) rheometer. In operation, a concentrated polymer solution or melt is sheared in the gap (h) between the two parallel plates of radius R (e.g., 2.5 cm) whose axes are offset by the distance a . The top plate is rotated at an angular frequency, ω (rad s⁻¹). Force can be measured in the orthogonal directions by means of transducers mounted in the plane of the bottom plate.

5.1.4 Dielectric Analysis

In place of a mechanical strain, viscoelastic response may be characterized by applying a time-dependent electric voltage to the sample. The voltage establishes an electrical field in the sample, which becomes electrically polarized. This means that any induced and permanent dipoles become oriented in the electric field. Polarization due to ionic conduction and the induction of a dipole moment of the molecule resulting from the distortion of the electron cloud of individual atoms is nearly instantaneous, while polarization due to the molecular motion and alignment of permanent dipoles in the electric field requires time. The polarization and ionic conduction result in the creation of a current whose amplitude depends upon frequency, temperature, and the dielectric properties of the material. As in the case of the stress response in dynamic-mechanical analysis, the frequency of the current is the same as the applied field but is shifted by the phase angle, δ . In dielectric analysis, the most important parameter for characterizing a sample is its *dielectric constant*, ϵ , which is defined next.

Theory. When a voltage (V) is applied across two electrodes between which a dielectric material is placed, a charge is established across the capacitor. This charge, Q (units of coulombs), is related to V and the capacitance (C) of the material (units of farads) as

$$Q = CV. \quad (5.82)$$

The capacitance may be expressed in terms of the capacitance of vacuum, C_0 , as

$$C = \varepsilon C_0 \quad (5.83)$$

where ε (dimensionless) is the dielectric constant, which is a function of temperature and time (or frequency). By definition, the dielectric constant for a vacuum is unity. The dielectric constant for air is only slightly higher at 1.0006, while that for water, which is capable of strong polarization, is 81 at room temperature and low frequency. Since polarization is time dependent, there is a *short-time* or *instantaneous response* for the dielectric constant, ε_U (or ε_0), that results from ion migration and induced polarization. The *long-time response*, ε_R (or ε_∞), represents the sum of contributions of the instantaneous response and the complete alignment of the permanent dipoles in the electric field.

The *charge density*, σ , is defined as

$$\sigma = \frac{Q}{A} \quad (5.84)$$

where A is the area of the plate electrodes. The charge density in the absence of a dielectric (i.e., a vacuum) between the electrodes is represented as σ_0 . This charge density is related to the *electric field*, E , which is defined as the ratio of the voltage across the capacitor and the distance between the electrodes as

$$E = \frac{V}{d}. \quad (5.85)$$

The relation between electric field and charge density is given by *Gauss's flux theorem*:

$$E = 4\pi\sigma_0. \quad (5.86)$$

As previously discussed, the polarization that is time dependent, $P(t)$, contains an instantaneous component, P_U , due to dipole induction:

$$\lim_{t \rightarrow 0} P(t) = P_U. \quad (5.87)$$

The separate time-dependent (dipole-orientation) contribution to polarization is indicated as $P_D(t)$, giving the total polarization as

$$P(t) = P_D(t) + P_U. \quad (5.88)$$

From the limiting conditions at long time,

$$\lim_{t \rightarrow \infty} P(t) = P_R \quad (5.89)$$

and

$$\lim_{t \rightarrow \infty} P_D(t) = P_D, \quad (5.90)$$

it follows that

$$P_R = P_D + P_U. \quad (5.91)$$

The polarization at infinite time, P_R , is related to the charge density as

$$\sigma = \sigma_o + P_R. \quad (5.92)$$

Since

$$\sigma = \epsilon_R \sigma_o \quad (5.93)$$

and (from eq. (5.86))

$$\sigma_o = \frac{E}{4\pi} \quad (5.94)$$

it follows that substitution of these equations into eq. (5.92) gives

$$\epsilon_R - 1 = \left(\frac{4\pi}{E} \right) P_R. \quad (5.95)$$

Substitution of eq. (5.91) into eq. (5.95) then gives

$$\epsilon_R - 1 = \left(\frac{4\pi}{E} \right) (P_D + P_U). \quad (5.96)$$

In analogy to the expression for polarization (eq. (5.91)), we may write

$$\epsilon_R = \epsilon_D + \epsilon_U \quad (5.97)$$

and (following eq. (5.95))

$$\epsilon_U - 1 = \left(\frac{4\pi}{E} \right) P_U. \quad (5.98)$$

The objective in the preceding development is to obtain expressions for the time dependency of the transient [i.e., $\varepsilon(t)$] or more commonly the dynamic [i.e., $\varepsilon(\omega, t)$] dielectric constant in response to a steady [i.e., $E(t)$] or oscillatory voltage [i.e., $E^*(\omega, t)$] applied to the electrodes. The approach is to assume that the time rate of change of the polarization is proportional to the magnitude of its displacement from its equilibrium value (P_R) as

$$\frac{dP(t)}{dt} = -\frac{P(t) - P_R}{\tau} \quad (5.99)$$

where τ is a time constant or relaxational time. From eq. (5.88), we may write

$$\frac{dP(t)}{dt} = \frac{dP_D}{dt}. \quad (5.100)$$

Substitution of eq. (5.100), eq. (5.88) for $P(t)$, and eq. (5.91) for P_R into eq. (5.99) gives

$$\frac{dP_D(t)}{dt} = -\frac{P_D(t) - P_D}{\tau}. \quad (5.101)$$

From eqs. (5.91), (5.95), and (5.98) it can be shown that

$$P_D = \frac{E}{4\pi} (\varepsilon_R - \varepsilon_U) \quad (5.102)$$

where $(\varepsilon_R - \varepsilon_U)$ is called the *dielectric relaxational strength*. Substitution of eq. (5.102) into eq. (5.101) and rearrangement gives the differential equation for a time-dependent electric field

$$\tau \frac{dP_D(t)}{dt} + P_D(t) = \frac{E(t)}{4\pi} (\varepsilon_R - \varepsilon_U). \quad (5.103)$$

For a frequency-dependent (i.e., sinusoidal) voltage

$$E^*(\omega, t) = E_0 \exp(i\omega t), \quad (5.104)$$

the differential equation of eq. (5.103) may be solved assuming that $t \gg \tau$, which indicates that steady-state conditions apply. The solution is given as

$$P_D^*(\omega) = \frac{(\varepsilon_R - \varepsilon_U)}{1 + i\omega\tau} \frac{E^*(\omega)}{4\pi}. \quad (5.105)$$

A complex dielectric constant may be defined in terms of real and imaginary components, in a similar manner to dynamic compliance, as

$$\varepsilon^* = \varepsilon' - i\varepsilon'' \quad (5.106)$$

where

$$\tan \delta_e = \frac{\varepsilon''}{\varepsilon'} . \quad (5.107)$$

With analogy to eq. (5.102) and recognizing that ε_R is the only frequency-dependent component of the dielectric constant, we can write

$$\varepsilon^*(\omega) = \frac{4\pi P_D^*(\omega)}{E^*(\omega)} + \varepsilon_U . \quad (5.108)$$

Rearranging this equation for $P_D^*(\omega)$ and substitution of this expression into eq. (5.105) gives

$$\varepsilon^*(\omega) = \varepsilon_U + \frac{\varepsilon_R - \varepsilon_U}{1 + i\omega\tau} . \quad (5.109)$$

Multiplication of the numerator and denominator of the second term on the RHS of eq. (5.109) by its complex conjugate allows the real and imaginary components of ε^* to be resolved as

$$\varepsilon^*(\omega) = \varepsilon_U + \left(\frac{\varepsilon_R - \varepsilon_U}{1 + i\omega\tau} \right) \times \left(\frac{1 - i\omega\tau}{1 - i\omega\tau} \right) = \varepsilon_U + \frac{\varepsilon_R - \varepsilon_U}{1 + \omega^2\tau^2} - i \frac{\omega\tau(\varepsilon_R - \varepsilon_U)}{1 + \omega^2\tau^2} . \quad (5.110)$$

Comparison of this equation with eq. (5.106) gives

$$\varepsilon' = \varepsilon_U + \frac{\varepsilon_R - \varepsilon_U}{1 + \omega^2\tau^2} \quad (5.111)$$

and

$$\varepsilon'' = \frac{\omega\tau(\varepsilon_R - \varepsilon_U)}{1 + \omega^2\tau^2} . \quad (5.112)$$

As in the case of dynamic-mechanical oscillation of a Maxwell model (see Problem 5.4b), it is easily shown that ε'' exhibits a maximum at a frequency equal to the reciprocal of the relaxation time, τ , as shown by the plot of ε' (eq. (5.111)), ε'' (eq. (5.112)), and $\tan \delta_e$ versus frequency in Figure 5-12.

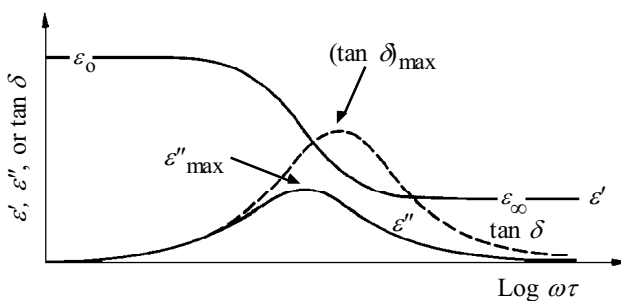


Figure 5-12 Illustration of the frequency dependence of the dielectric constant.

Equations (5.111) and (5.112) give a reasonable qualitative behavior of experimental ϵ' and ϵ'' with the limitation that the phenomenological model utilizes a single relaxation time, τ , whereas a distribution of relaxation times would be expected for high polymers. From the early work of Peter Debye, there have been a number of attempts to relate macroscopic properties of the dielectric, such as ϵ and P , with molecular properties, such as the dipole moment or molecular polarizability. A full description of these approaches is beyond the scope of this text, and the reader is encouraged to look at other reference sources such as the book by Daniels listed in Suggested Reading at the end of the chapter.

Experimental Methods. Values ϵ' and ϵ'' can be readily measured for polymer solutions, melts, and films over a wide range of frequencies (10^{-4} to 10^{10} Hz) by a variety of techniques. As a result of this wide frequency range, dielectric data can be plotted against frequency (i.e., frequency-plane measurements) at constant temperature in comparison with the temperature-plane plots typical for dynamic-mechanical measurements.

In the case of solid samples, a polymer film may be coated with an electrically conductive layer of gold or other metal to improve contact with the electrodes. The film is then placed in an electrode cell and immersed in a constant-temperature bath. The cell is connected to a frequency generator and typically to an electrical bridge to measure the electrical impedance of the sample. Frequently, a Schering impedance bridge, such as the one illustrated in Figure 5-13, is used over a frequency range from about 1 Hz to 10 MHz. A Schering bridge is similar to a Wheatstone bridge except that impedance, rather than resistance, is measured. By balancing the bridge, the equivalent capacitance, C_x , and resistance, R_x , of the sample are obtained. The parameters $\tan \delta_e$, ϵ' , and ϵ'' can then be determined as

$$\tan \delta = R_x C_x \omega, \quad (5.113)$$

$$\varepsilon' = \frac{C_x}{C_o(1 + \tan^2 \delta_e)}, \quad (5.114)$$

and

$$\varepsilon'' = \varepsilon' \tan \delta_e. \quad (5.115)$$

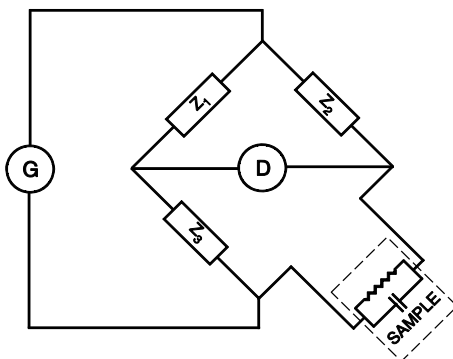


Figure 5-13 Representation of a dielectric test facility, a Schering bridge, that includes a frequency generator (G) and null detector (D). One or several of the bridge impedances are adjusted in order that the magnitude and the phase of the voltage drops across Z_1 and Z_2 are zero.

A plot of dielectric-loss (ε'') data for a polycarbonate sample as a function of frequency over a wide range of temperatures is shown in Figure 5-14A and B. In general, the glass-transition and secondary-relaxation processes can be investigated by dielectric measurements provided that there is polarizability in the side groups or main-chain repeating units. Dielectric measurements have also been used to study the cure process in thermoset composites by measurement of the dielectric constant at fixed frequency and temperature as a function of time.

Thermally Stimulated Current Analysis. Thermally stimulated current (TSC) analysis is a method related to dielectric spectroscopy that can be used to investigate amorphous transitions. In this technique, polymer dipoles are first oriented by applying a high potential across the sample at elevated temperatures (typically above T_g). The orientation is frozen by dropping the temperature below expected transitions while the potential is maintained. Next, the electric field is removed and the sample is heated. As the dipoles reorient, the resulting electric current due to the depolarization is measured as a function of temperature. Maxima appear at each transition due to the increased molecular mobility as temperature is increased. The resulting plot of thermally stimulated current against temperature is

very similar to that of the dynamic-mechanical loss data and can be used to identify secondary relaxations and glass transitions.

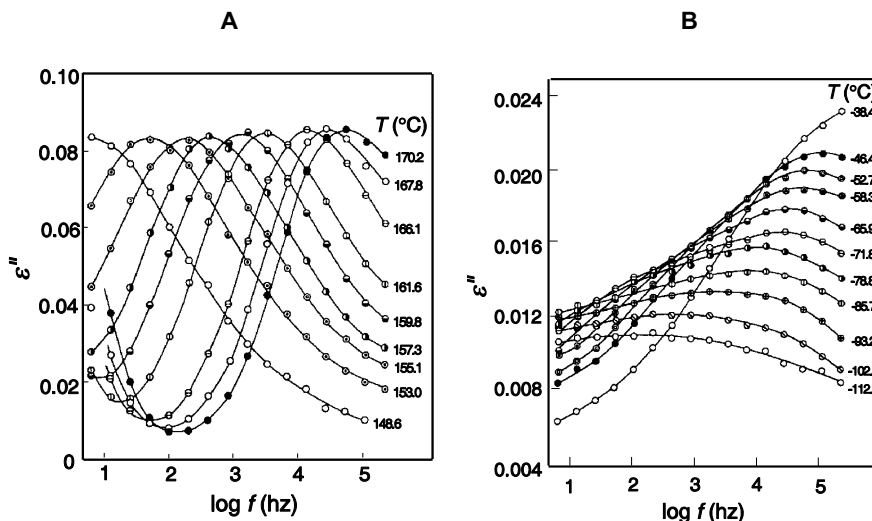


Figure 5-14 Plots of the dielectric loss constant (ϵ'') of polycarbonate as a function of frequency at different temperatures [11]. **A.** High-temperature data showing the α peak (i.e., the glass transition). **B.** Low-temperature data showing the secondary γ relaxation. The peak maxima are shown to increase in frequency with increasing temperature.

5.1.5 Dynamic Calorimetry

A variation of traditional differential scanning calorimetry (Section 4.3.2) is temperature-modulated DSC (TMDSC) [12, 13]. The principle behind TMDSC is the superimposition of a sinusoidal modulation of temperature upon the constant heating (or cooling) rate of conventional DSC operation. The sample temperature, T , is then given by

$$T = T_o + q_o t + A_T \sin(\omega t) \quad (5.116)$$

where T_o is the initial temperature for the modulated scan, q_o is the average heating rate, A_T is the amplitude of the temperature modulation, and ω is the angular frequency (rad min^{-1}) of the modulation. The time derivative of eq. (5.116) gives the heating rate modulation

$$q = q_o + A_T \omega \cos(\omega t). \quad (5.117)$$

Fourier transformations of the modulated heating rate (q) and the heat-flow (HF) signals yield the average values $\langle q \rangle$ and $\langle HF \rangle$, the amplitudes A_q and A_{HF} of the heating rate and heat-flow signals, and the phase angle, ϕ , between these signals. From these values, average and complex heat capacities are obtained as

$$\langle C_p \rangle = \frac{\langle HF \rangle}{\langle q \rangle} \quad (5.118)$$

and

$$C_p^* = C_p' - iC_p'' . \quad (5.119)$$

The magnitude of the complex heat capacity is determined from the signal amplitudes as

$$|C_p^*| = \frac{A_{HF}}{A_q} . \quad (5.120)$$

The real (i.e., in-phase), C_p' , and imaginary (i.e., out-of-phase), C_p'' , components of the complex heat capacity are related to the magnitude and phase angle as

$$C_p' = |C_p^*| \cos \phi \quad (5.121)$$

and

$$C_p'' = |C_p^*| \sin \phi . \quad (5.122)$$

These dynamic components of heat capacity are shown in comparison to a conventional DSC signal in Figure 5-15. In the TMDSC scan, the glass transition is identified by both a step change in C_p' and a peak in C_p'' in a manner similar to dielectric spectroscopy. In a conventional DSC scan, T_g is usually identified as the point of inflection in the specific heat or heat flow signal and is dependent upon the heating (or cooling) rate (see Section 4.3.4). In contrast, T_g determined from TMDSC measurements, like T_g determined by other dynamic techniques, is dependent upon the frequency of the modulation.

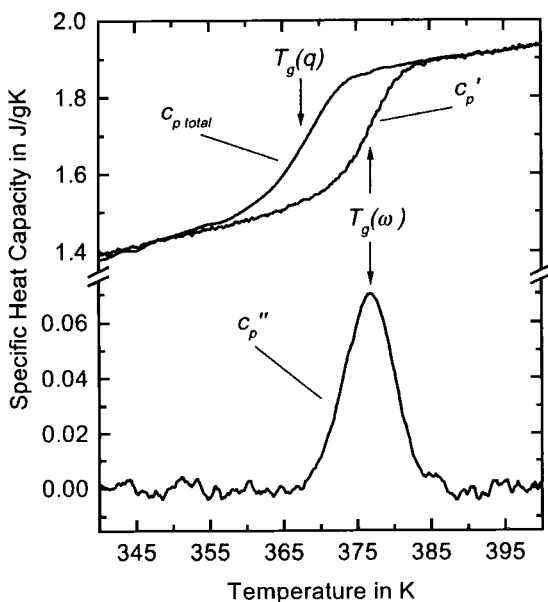


Figure 5-15 TMDSC scan of a polystyrene sample ($q_0 = -0.25 \text{ K min}^{-1}$; $A_T = 0.5 \text{ K}$, period $t_p = 60 \text{ s}$). A conventional DSC scan is shown by the top curve ($C_{p,\text{total}}$). Reprinted from S. Weyer, M. Merzlyakov, and C. Schick, *Application of an Extended Tool–Narayanaswamy–Moynihan Model. Part 1. Description of Vitrification and Complex Heat Capacity Measured by Temperature-Modulated DSC*. Thermochimica Acta, 2001. **377**: p. 85–96. Copyright 2001, with permission from Elsevier Science.

Alternatively, the response of TMDSC can be expressed as reversing and non-reversing heat flow as

$$\langle HF \rangle_{\text{rev}} = |C_p *| q_0 \quad (5.123)$$

and

$$\langle HF \rangle_{\text{non-rev}} = \langle HF \rangle - \langle HF \rangle_{\text{rev}}. \quad (5.124)$$

For isothermal operation ($q_0 = 0$), as may be used in the study of thermoset cure, the reversing heat flow is zero (eq. (5.123)) and the non-reversing heat flow is the same as the total heat flow. One of the advantages of TMDSC has been its potential to separate reversible processes, such as the pseudo second-order glass transition, from non-reversing events (e.g., enthalpy recovery, recrystallization, and chemical reac-

tion occurring during cure). Exothermal events are detected only during the non-reversing signal.

5.1.6 Time–Temperature Superposition

Often, it is important to know how a material will behave (e.g., creep or stress relaxation) at a fixed temperature, but over a long time period (perhaps years) that may not be realistically accessible. Fortunately, long-time behavior can be evaluated by measuring stress-relaxation or creep data over a shorter period of time but at several different temperatures. Information from each of these different temperature curves may then be combined to yield a *master curve* at a single temperature by horizontally shifting each curve along the log time scale. This technique is called *time–temperature superposition* and is a foundation of linear viscoelasticity theory. In this procedure, the master curve is plotted as stress-relaxation modulus or creep compliance versus reduced time, t/a_T . The *shift factor*, a_T , is defined as the ratio of (real) time to reach a particular value of modulus at some temperature to the reference-scale time coordinate, t_r , corresponding to the same value of modulus in the master curve at the reference temperature, T_r ,

$$a_T = \frac{t}{t_r}. \quad (5.125)$$

Stated more concisely, the time–temperature superposition principle says that

$$E(T, t) = E(T_r, t_r). \quad (5.126)$$

The procedure of horizontal shifting is illustrated for stress-relaxation and torsional-creep data for polycarbonate in Figure 5-16.

The dependence of the shift factor, a_T , on temperature is given by the *Williams–Landel–Ferry (WLF) relationship*

$$\log a_T = \frac{-C_1(T - T_r)}{C_2 + T - T_r} \quad (5.127)$$

where C_1 and C_2 are constants for a given polymer and T_r is the reference temperature. When T_r is taken to be the polymer T_g , as it often is, C_1 and C_2 may be approximated by the “universal” values of 17.44 and 51.6, respectively; however, significant deviations from these values may exist for some polymers (see Problem 5.7), as shown by values given for some common polymers in Table 5-3.

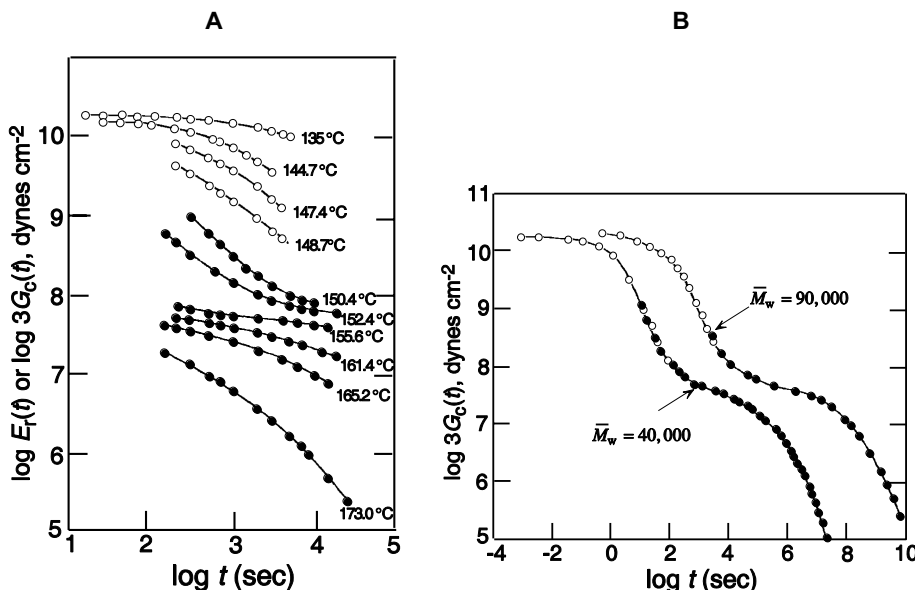


Figure 5-16 A. Modulus of polycarbonate ($\bar{M}_w = 90,000$) as a function of time and temperature from stress-relaxation (●) and torsional-creep (○) measurements. B. Resulting master curve obtained by shifting both sets of data at a reference temperature of 150°C and for two different molecular-weight samples of polycarbonate ($\bar{M}_w = 40,000$ and 90,000). The master curve is shown to shift to higher times with increasing molecular weight. J. P. Mercer, et al., *Viscoelastic Behavior of the Polycarbonate of Bisphenol A*. Journal of Applied Polymer Science, 1965. 9: p. 447–459.

Table 5-3 WLF Parameters of Some Common Polymers

Polymer	T_g (K)	C_1	C_2
Natural rubber	200	16.7	53.6
Polyisobutylene	202	16.6	104
Polyurethane	238	15.6	32.6
Poly(vinyl acetate)	304	17.4	43.4
Poly(ethyl methacrylate)	335	17.6	65.5
Poly(ethylene terephthalate), amorphous	343	17.1	31.7
Poly(ethylene terephthalate), crystalline	353	30.4	106.6
Poly(vinyl chloride)	353	16.2	49.7
Polystyrene	373	13.7	50.0

If C_1 and C_2 are not known, each curve may be horizontally shifted to the reference temperature curve until a value of modulus on the shifted curve coincides

with one on the reference curve.* The shift factor may then be calculated by use of the defining relationship for a_T given by eq. (5.125). The WLF parameters, C_1 and C_2 , may then be determined by plotting $(T - T_r)/\log a_T$ versus $(T - T_r)$, where rearrangement of eq. (5.127) gives

$$\frac{T - T_r}{\log a_T} = -\frac{1}{C_1}(T - T_r) - \frac{C_2}{C_1}. \quad (5.128)$$

Following this procedure, C_1 is obtained directly from the inverse of the slope, and C_2 can then be calculated from the value of C_1 and the intercept (C_2/C_1). It can be shown that C_1 and C_2 can be related to the fractional free volume at T_g (f_g) and the thermal-expansion coefficient of free volume (see Chapter 11, Appendix A.1).

As discussed in Section 4.1.2, Gibbs and DiMarzio have suggested that a true second-order transition should occur at a temperature (T_2) where the conformational entropy is zero. This would occur at an *equilibrium* glassy state that conceptually can be obtained by cooling from the melt at an infinitely slow rate. Therefore, the WLF relation can be used to determine the relationship between the thermodynamic transition temperature and the kinetic T_g by noting that shifting from a finite to an infinite time scale requires that the shift factor approach infinity or that the denominator in eq. (5.127) go to zero, where $T_r = T_g$ and $T = T_2$. This means that

$$T_2 = T_g - C_2 \approx T_g - 52 \quad (5.129)$$

using the universal value for C_2 . In other words, the true second-order transition temperature should lie approximately 52°C *below* the experimentally measured T_g .

The master curve for stress-relaxation modulus, shown in Figure 5-16B, illustrates the four characteristic regions of a high-molecular-weight polymer. At short times, the polymer behaves as a glassy material (glassy plateau), while at longer times the modulus sharply drops to the rubbery-plateau region. At sufficiently long times, the stress-relaxation modulus again rapidly falls. Conceptually, what is happening is that initially the polymer chains are entangled and unable to fully accommodate the applied strain on the sample. This results in a high apparent modulus. Eventually, sufficient time has elapsed at the experimental temperature for the chains to slip, and the sample adjusts to the load. The form of the master curve for stress relaxation is qualitatively similar to that of the plot of Young's modulus in

* It may be shown that for elastic chains in a network, the shear modulus is proportional to temperature and to density (i.e., chain concentration). Therefore, it may be necessary to introduce a small vertical shift to account for the dependence of modulus on both temperature and density (ρ). This correction may be expressed as

$$E(T_r, t_r) = \frac{\rho(T_r) T_r}{\rho(T) T} E(T, t).$$

Figure 4-19 where the units of the abscissa were temperature rather than time. The fact that time and temperature can be superimposed means that the change in modulus of the material with increasing time at constant temperature is equivalent to the change in modulus when measured at identical times but at increasing temperature.

5.1.7 Boltzmann Superposition Principle

Tensile (or shear) modulus and tensile (or shear) compliance are inversely related (see eq. 4.46). The same is true for complex modulus and complex compliance (see eq. (5.17)), but creep-compliance and stress-relaxation moduli are not as simply related; that is,

$$D(t) \neq \frac{1}{E_r(t)}.$$

This is because creep-compliance and stress-relaxation moduli are obtained by distinctly different experimental procedures. As discussed in Chapter 4, a fixed *load* is applied instantly at $t = 0$ in a creep experiment, while a fixed *strain* is applied instantaneously at $t = 0$ for stress-relaxation measurements.

A relationship between the creep-compliance and stress-relaxation moduli can be established by application of another fundamental statement of linear viscoelasticity, the *Boltzmann superposition principle*. This Boltzmann superposition principle states that the *total strain is a linear function of total applied stress*. In the case of a creep experiment, the strain is a function of the total load (stress) history in which each load makes an independent contribution to the creep. If a load, σ_o , is instantaneously applied at time $t = 0$ and a second load, σ_i , is applied at time $t = u_i$, as illustrated in Figure 5-17, then the strain at some time t' , where $t' > u_i$, is given by the Boltzmann superposition principle as

$$\varepsilon(t') = \sigma_o D(t') + \sigma_i D(t' - u_i). \quad (5.130)$$

In the general case of the application of a series of discrete loads, $\sigma_1, \sigma_2, \dots, \sigma_n$, applied at times $t = u_1, u_2, \dots, u_n$, the total resulting strain response in creep deformation is calculated from the tensile compliance function, $D(t)$, as

$$\varepsilon(t) = \sum_{i=1}^n \sigma_i D(t - u_i). \quad (5.131)$$

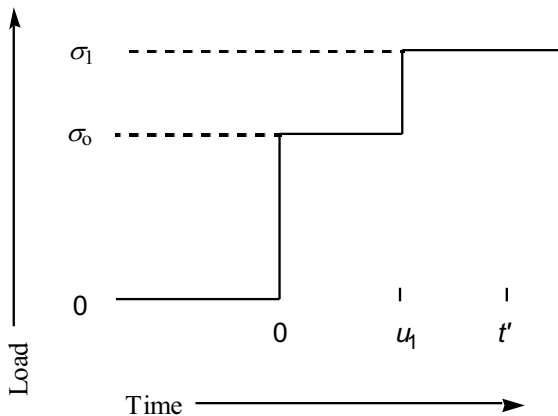


Figure 5-17 Stress history corresponding to the strain response given by eq. (5.130).

If the applied stress is some *continuous* function of time, $\sigma(t)$, application of the Boltzmann superposition principle gives the creep response in integral form as

$$\varepsilon(t) = \int_{-\infty}^t \left[\frac{\partial \sigma(u)}{\partial u} \right] D(t-u) du \quad (5.132)$$

where u is the time variable and integration covers the entire stress history ($-\infty < u \leq t$) of the sample. Using a convenient variable change, $a = t - u$, integration of eq. (5.132) by parts (see Appendix E at the end of this text) gives

$$\varepsilon(t) = D(0)\sigma(t) + \int_0^\infty \sigma(t-a) \left[\frac{\partial D(a)}{\partial a} \right] da. \quad (5.133)$$

The corresponding equations for stress relaxation are

$$\sigma(t) = \int_{-\infty}^t \left[\frac{\partial \varepsilon(u)}{\partial u} \right] E(t-u) du \quad (5.134)$$

and

$$\sigma(t) = E(0)\varepsilon(t) + \int_0^\infty \varepsilon(t-a) \left[\frac{\partial E(a)}{\partial a} \right] da. \quad (5.135)$$

5.1.8 Interrelationships between Transient and Dynamic Properties

A basis for relating the creep-compliance and stress-relaxation moduli is obtained by taking the Laplace transform of eqs. (5.132) and (5.134). A summary of the principles and basic relationships of Laplace transforms is included in Appendix E. It can be shown that the transformations of eqs. (5.132) and (5.134) give

$$\mathcal{L}[\varepsilon(t)] = p\mathcal{L}[\sigma(t)]\mathcal{L}[D(t)] \quad (5.136)$$

and

$$\mathcal{L}[\sigma(t)] = p\mathcal{L}[\varepsilon(t)]\mathcal{L}[E(t)] \quad (5.137)$$

where p is the Laplace variable. Substitution of eq. (5.136) into the RHS of eq. (5.137) gives the relationship between creep-compliance and stress-relaxation moduli in *transform space* (see Problem 5.3) as

$$\frac{1}{p^2} = \mathcal{L}[D(t)]\mathcal{L}[E(t)]. \quad (5.138)$$

The Boltzmann superposition principle also provides a means of interrelating dynamic (moduli) and transient (stress-relaxation) data. Utilizing eq. (5.134) and making a variable change in the form $s = t - u$ give

$$\sigma(t) = - \int_0^\infty \left[\frac{\partial \varepsilon(t-s)}{\partial s} \right] E(s) ds. \quad (5.139)$$

In dynamic oscillation,

$$\varepsilon(t-s) = \varepsilon^\circ \exp[i\omega(t-s)] \quad (5.140)$$

and

$$\frac{\partial \varepsilon(t-s)}{\partial s} = \varepsilon(t)(-i\omega) \exp(-i\omega s). \quad (5.141)$$

Substitution of these equations into the integral of eq. (5.139), and noting that $\varepsilon(t)$ is not a function of s and, therefore, can be taken outside the integral, gives

$$\sigma(t) = i\varepsilon(t) \int_0^\infty \omega \exp(-i\omega s) E(s) ds. \quad (5.142)$$

Dividing both sides of this equation by $\varepsilon(t)$ and replacing the complex term by Euler's identity [$\exp(-i\omega s) = \cos \omega s - i \sin \omega s$] give the complex modulus as

$$E^* = \frac{\sigma(t)}{\varepsilon(t)} = \int_0^\infty \omega \sin(\omega s) E(s) ds + i \int_0^\infty \omega \cos(\omega s) E(s) ds. \quad (5.143)$$

Relating this equation to the customary form of E^* ($= E' + iE''$) gives the relationships between the stress-relaxation modulus, $E(s)$, and the storage and loss moduli as

$$\boxed{E' = \omega \int_0^\infty \sin(\omega s) E(s) ds} \quad (5.144)$$

and

$$\boxed{E'' = \omega \int_0^\infty \cos(\omega s) E(s) ds}. \quad (5.145)$$

The preceding equations may be recognized as the Fourier *sine* and *cosine* transforms of the stress-relaxation modulus function. This means that if the form of the stress-relaxation function is known, the dynamic moduli can be determined by taking the sine or cosine transforms of the function. Tables of these transforms are available in most handbooks of mathematical tables. For convenience, some important Fourier transforms are listed in Appendix E.

5.2 Introduction to Rubber Elasticity

In 1805, John Gough observed that the temperature of a rubber band would increase as it is stretched adiabatically. Also, if a weight is hung from the end of the rubber band and heat is applied, the rubber band will *decrease* in length rather than stretch, as observed for other materials such as common metals and gases as illustrated in Figure 5-18. It was not until the 1930s that an explanation for this behavior, known as the *Gough-Joule effect*, was provided by means of classical thermodynamics as described in the following section.

5.2.1 Thermodynamics

The first and second laws of thermodynamics applied to a reversible, equilibrium process provide the relationship between internal energy (U), entropy (S), and work (W) as

$$dU = TdS - dW. \quad (5.146)$$

For deformation of a rubber band, the work is a combination of pressure-volume expansion and the work due to the (tensile) force (f) applied to the rubber band, given as

$$dW = pdV - f d\ell \quad (5.147)$$

where the convention is that work done *by* the system (i.e., pressure-volume work) is positive and the work done *on* the system (i.e., force-displacement work) is negative. Enthalpy is related to the internal energy as

$$dH = dU + pdV. \quad (5.148)$$

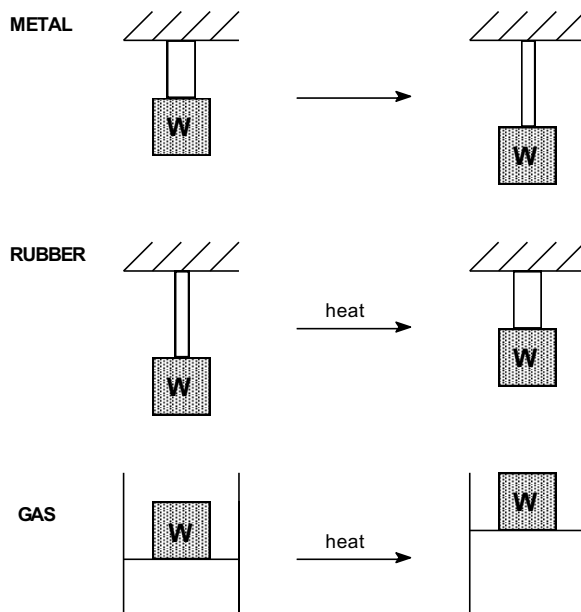


Figure 5-18 Illustration of the effect of heat on metal, rubber, and gas. Shaded boxes represent an applied load. Used with permission from J. E. Mark, *Rubber Elasticity*. The Journal of Chemical Education. **58**(11): 1981, p. 898–903. Copyright © 1981, Division of Chemical Education, Inc., American Chemical Society.

Substitution of eqs. (5.146) and (5.147) (in the form $pdV = dW + f d\ell$) into eq. (5.148) gives

$$dH = TdS + f d\ell. \quad (5.149)$$

At constant temperature and pressure, rearrangement of eq. (5.149) in terms of force and taking the (partial) derivative with respect to length at constant temperature and pressure give

$$f = \left(\frac{\partial H}{\partial \ell} \right)_{T,p} - T \left(\frac{\partial S}{\partial \ell} \right)_{T,p}. \quad (5.150)$$

Equation (5.150) shows that elastic force has both an enthalpic and entropic component ($f = f_e + f_s$).

In order to obtain an expression for the temperature dependence of force, we make use of the relation*

$$\left(\frac{\partial S}{\partial \ell} \right)_{T,p} = - \left(\frac{\partial f}{\partial T} \right)_{p,\ell}. \quad (5.151)$$

Substitution of eq. (5.151) into eq. (5.150) gives

$$f = \left(\frac{\partial H}{\partial \ell} \right)_{T,p} + T \left(\frac{\partial f}{\partial T} \right)_{p,\ell}. \quad (5.152)$$

Rearrangement of eq. (5.152) gives

$$\left(\frac{\partial f}{\partial T} \right)_{p,\ell} = \frac{f - (\partial H / \partial \ell)_{T,p}}{T}. \quad (5.153)$$

Equation (5.153) indicates that the slope of a force-temperature plot will be positive, as is usually observed for elastomers at moderate or higher extension, if

$$f > \left(\frac{\partial H}{\partial \ell} \right)_{T,p}.$$

This condition is satisfied except for very small extensions, as illustrated by Figure 5-19. It can be shown that the change of enthalpy due to deformation at constant temperature and pressure has both internal energy, U , and volume contributions as given by the expression

* Obtained from the reciprocity relationship for the exact differential equation for Gibbs free energy given as

$$dG = -SdT + Vdp + fd\ell.$$

$$\left(\frac{\partial H}{\partial \ell} \right)_{T,p} = \left(\frac{\partial U}{\partial \ell} \right)_{T,V} + T \left(\frac{\alpha}{\beta} \right) \left(\frac{\partial V}{\partial \ell} \right)_{T,p}. \quad (5.154)$$

Since elastomers are nearly incompressible, it is clear that the second term on the RHS of eq. (5.154) is very small. Furthermore, changes in internal energy due to conformation changes during deformation are also small. For these reasons, enthalpic contributions in rubber elasticity are generally insignificant and rubber-like behavior can be satisfactorily explained on the basis of entropic considerations alone. Conceptually, we can view polymer chains to be in an entropically favorable, disordered state when undeformed. During deformation, the chains become ordered and, therefore, an entropically driven force develops to restore the more favorable disordered conformational state.

The importance of entropy to the deformation of an ideal elastomer can be compared to that of an ideal gas. Heating a gas increases the driving force toward a state of maximum entropy. This means that an increase in temperature results in an increase in volume at constant pressure as was illustrated in Figure 5-18. Since the deformation of a compressed gas can be expressed as the reciprocal volume ($1/V$), we can say that an increase in the temperature of a gas at constant pressure results in a decrease in its deformation. This is analogous to the case of an elastomer whose measure of deformation is its length (ℓ), which decreases with an increase in temperature.

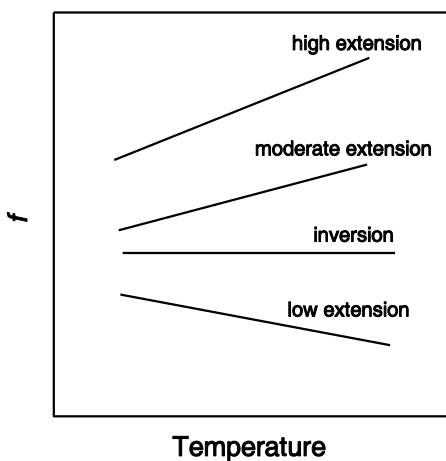


Figure 5-19 Thermoelastic behavior of elastomer at various elongations.

5.2.2 Statistical Theory

In the 1920s, Staudinger developed a thermodynamic expression for elastic force based upon polymer-chain statistics. The elastic force is related to the Helmholtz free energy, A , as

$$f = \left(\frac{\partial \Delta A}{\partial \ell} \right)_{T,V} \quad (5.155)$$

where $A = U - TS$ and ΔA represents the difference in Helmholtz free energy between the deformed and undeformed network ($\Delta A = A_d - A_u$). The entropy contribution is linked to the total number of conformations, Ω , available to the rubber network through the Boltzmann relation $S = k \ln \Omega$. An expression for Ω is obtained from the Gaussian radial-distribution function $\omega(r)$ for the i th chain in a network of N chains (see Section 3.1, eq. (3.5) and Figure 3-2) as

$$\Omega = \prod_{i=1}^N \omega(r_i). \quad (5.156)$$

The resulting equation for force is usually given in the form

$$f^* = G_o \left(\lambda - \frac{1}{\lambda^2} \right) \quad (5.157)$$

where f^* is the (nominal) stress, G_o is the shear modulus (one-third of the tensile modulus for incompressible materials), and λ is the principal *extension ratio*

$$\lambda = \frac{L}{L_o} = 1 + \varepsilon \quad (5.158)$$

where L_o is the original (undeformed) length of the elastomer and ε is the engineering or nominal strain.

The shear modulus, G_o , is proportional to temperature and to the number of chains in the elastomeric network (see eq. (4.49)). High crosslink density results in an increase in the number of network chains per unit volume and will, therefore, increase modulus. This will become apparent by comparing the stiffness of a lightly crosslinked rubber band with a highly crosslinked ebonite bowling ball.

As shown in Figure 5-20, the theory gives a good representation of the experimental stress-strain curve only for moderate strains ($\lambda = 1.5$). For larger extensions, the theory overestimates stress because the conformational state is no longer adequately predicted by the Gaussian-distribution model used in the derivation (eq. (5.156)). At still higher extensions ($\lambda > 6$), the observed stress rapidly rises due to the development of strain-induced crystallization. The increase in modulus is due to

the physical reinforcement effect of the crystallites. In general, the increase in modulus of an elastomer due to the presence of crystallites or the incorporation of fillers such as carbon black can be approximated by the *Guth–Smallwood equation*

$$\frac{E_f}{E_o} = 1 + 2.5\phi_f + 14.1\phi_f^2 \quad (5.159)$$

where E_f is the tensile (Young's) modulus of the filled elastomer, E_o is the modulus of the unreinforced elastomer, and ϕ_f is the volume fraction of the filler.

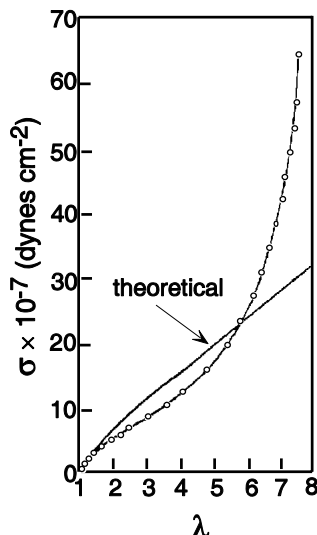


Figure 5-20 Comparison of the statistical-thermodynamic relationship (eq. (5.157) where $G_o = 4 \times 10^6$ dynes cm^{-2}) with the experimental stress-strain data (\circ) for natural rubber. Adapted from L. R. G. Treloar, *Stress-Strain Data for Vulcanized Rubber under Various Types of Deformation*. Transactions of the Faraday Society, 1944. **40**: p. 59.

5.2.3 Phenomenological Model

Another widely used model of rubber elasticity has its origin in continuum mechanisms. It is known as the *Mooney–Rivlin equation*, given as

$$f^* = 2 \left(C_1 + \frac{C_2}{\lambda} \right) \left(\lambda - \frac{1}{\lambda^2} \right) \quad (5.160)$$

where C_1 and C_2 are empirical constants (distinct from the WLF constants) and f^* is given as

$$f^* = \frac{f}{A_d} \quad (5.161)$$

where A_d is the cross-sectional area of the undeformed elastomer. Values of C_1 and C_2 are obtained by plotting experimental stress-strain data in terms of the *reduced stress* [f^*] defined as

$$[f^*] = \frac{f^*}{\lambda - \lambda^{-2}} \quad (5.162)$$

versus $1/\lambda$. The intercept gives C_1 while the slope yields C_2 . Equation (5.160) is very useful for describing the stress-strain curves of elastomers over a wide range of extensions.

5.2.4 Recent Developments

The statistical theory of rubber elasticity is based upon a number of significant assumptions including:

- Crosslinking does not alter the chain dimensions from their unperturbed state.
- The end-to-end separation of network chains can be fit by a Gaussian distribution.
- Crosslink junctions are fixed at their mean positions and these junctions deform in the same ratio as the macroscopic deformation of the sample (i.e., *affine deformation*).

An alternative to the affine model is the “*phantom chain*” approximation whereby chains are permitted to pass through one another as if they had zero cross-sectional area. While the deformation of the mean position of the crosslink junctions is affine, the junctions are allowed to fluctuate about their mean positions. The phantom theory predicts moduli that are lower than predicted by the affine model. Both models predict that the modulus of a rubber network is independent of the deformation; however, experiments show that modulus actually decreases with an increase in λ as is correctly represented by the Mooney–Rivlin equation (eq. (5.160)), which owes its origin to continuum mechanics. Comparison of eq. (5.160) with the form of the statistical-theory result (eq. (5.157)) indicates that the λ -dependence of modulus is given as

$$[f^*] = 2C_1 + 2C_2\lambda^{-1} \quad (5.163)$$

where the Mooney–Rivlin constants are themselves independent of λ . More recent theoretical models, which are beyond the scope of this discussion, provide an improved model for the dependence of $[f^*]$ on λ and offer better insight into the molecular theory of rubber elasticity [14]. These include the constrained-junction and, later, the constrained-chain models for which the phantom-model prediction is approached as a limiting case at small deformations.

SUGGESTED READING

DIELECTRIC SPECTROSCOPY

- Daniels, V. V., *Dielectric Relaxation*. 1967, London: Academic Press.
Runt, J. P., and J. J. Fitzgerald, *Dielectric Spectroscopy of Polymeric Materials: Fundamentals and Applications*. 1997, Washington DC: American Chemical Society.

DYNAMIC MECHANICAL SPECTROSCOPY

- Boyer, R. F., *Dependence of Mechanical Properties on Molecular Motion in Polymers*. Polymer Engineering and Science, 1968. **8**(3): p. 161.
Gillham, J. K., *Characterization of Thermosetting Materials by Torsional Braid Analysis*. Polymer Engineering and Science, 1976. **16**(5): p. 353.
Gillham, J. K., *The TBA Torsion Pendulum: A Technique for Characterizing the Cure and Properties of Thermosetting Systems*. Polymer International, 1997. **44**: p. 262.
Gillham, J. K., and J. B. Enns, *On the Cure and Properties of Thermosetting Polymers Using Torsional Braid Analysis*. Trends in Polymer Science, 1994. **2**(12): p. 406.
Heijboer, J., *The Torsion Pendulum in the Investigation of Polymers*. Polymer Engineering and Science, 1979. **19**(10): p. 664.

RUBBER ELASTICITY

- Boyce, M. C., and E. M. Arruda, *Constitutive Models of Rubber Elasticity: A Review*. Rubber Chemistry and Technology, 2000. **73**: p. 504.
Erman, B., and J. E. Mark, *Rubber-Like Elasticity*. Annual Review of Physical Chemistry, 1989. **40**: p. 351.
Flory, P. J., *Molecular Theory of Rubber Elasticity*. Polymer Journal, 1985. **17**(12): p. 1.
James, H. M., and E. Guth, *Simple Presentation of Network Theory of Rubber, with a Discussion of Other Theories*. Journal of Polymer Science, 1949. **4**: p. 153.
Kloczkowski, A., *Application of Statistical Mechanics to the Analysis of Various Physical Properties of Elastomeric Networks—a Review*. Polymer, 2002. **43**: p. 1503.
Mark, J. E., *Rubber Elasticity*. Journal of Chemical Education, 1981. **58**(11): p. 898.
Mark, J. E., *Experimental Determinations of Crosslink Densities*. Rubber and Chemistry Technology, 1982. **55**(13): p. 762.
Mark, J. E., and B. Erman, *Rubberlike Elasticity*. 1988, New York: John Wiley & Sons.

- Mark, J. E., and B. Erman, *Elastomeric Polymer Networks*. 1992, Englewood Cliffs: Prentice Hall.
- Nielsen, L. E., *Cross-Linking Effect on Physical Properties of Polymers*. Journal of Macromolecular Science—Reviews in Macromolecular Chemistry, 1969. C3(1): p. 69.
- Treloar, L. R. G., *Stress-Strain Data for Vulcanised Rubber under Various Types of Deformation*. Transactions of the Faraday Society, 1944. 40: p. 59.
- Treloar, L. R. G., *The Physics of Rubber Elasticity*. 1958, Oxford University Press.

TEMPERATURE-MODULATED DSC

- Hutchinson, J. M., and S. Montserrat, *The Application of Temperature-Modulated DSC to the Glass Transition Region. II. Effect of a Distribution of Relaxation Times*. Thermochimica Acta, 2001. 377: p. 63–84.
- Montserrat, S., and I. Cima, *Isothermal Curing of an Epoxy Resin by Alternating Differential Scanning Calorimetry*. Thermochimica Acta, 1999. 330: p. 189–200.
- Ribeiro, M., and J.-P. E. Grolier, *Temperature Modulated DSC for the Investigation of Polymer Materials*. Journal of Thermal Analysis and Calorimetry, 1999. 57: p. 253–263.
- Scherrenberg, R., V. Mathot, and P. Steeman, *The Applicability of TMDSC to Polymeric Systems. General Theoretical Description Based on the Full Heat Capacity Formulation*. Journal of Thermal Analysis, 1998. 54: p. 477–499.
- Scherrenberg, R., V. Mathot, and A. Van Hemelrijck, *The Practical Applicability of TMDSC to Polymeric Systems*. Thermochimica Acta, 1999. 330: p. 3–19.

VISCOELASTICITY

- Aklonis, A. A., and W. J. MacKnight, *Introduction to Polymer Viscoelasticity*. 2nd ed. 1983, New York: John Wiley & Sons.
- Ferry, J. D., *Viscoelastic Properties of Polymers*. 3rd ed. 1980, New York: John Wiley & Sons.
- Ferry, J. D., *Some Reflections on the Early Development of Polymer Dynamics: Viscoelasticity, Dielectric Dispersion, and Self-Diffusion*. Macromolecules, 1991. 24(19): p. 5237–5245.
- McCrum, N. G., B. E. Read, and G. Williams, *Anelastic and Dielectric Effects in Polymeric Solids*, 1967, New York: John Wiley & Sons.
- Pearson, D. S., *Recent Advances in the Molecular Aspects of Polymer Viscoelasticity*. Rubber Chemistry and Technology, 1967. 40: p. 439.
- Tschoegl, N. W., *The Phenomenological Theory of Linear Viscoelastic Behavior: An Introduction*, 1989, Berlin: Springer-Verlag.

PROBLEMS

- 5.1** Show that $|E^*| = \sigma^\circ / \varepsilon^\circ$ and $|D^*| = 1/E^*$.

5.2 Show that the work per cycle per unit volume performed during dynamic tensile oscillation of a viscoelastic solid may be given as $\pi\sigma^o\varepsilon^o \sin\delta$ (eq. (5.30)).

5.3 Given the expression $G(t) = G_o \exp(-t/\tau) + G_i$, show that the compliance function, $J(t)$, can be written in the form $J(t) = A - B \exp(-C t/\tau)$, where A, B, and C are constants.

5.4 For a Maxwell model, show the following:

(a) The equation for complex modulus E^* (eq. (5.57)) can be obtained from the Fourier transform of the stress-relaxation modulus, E_r (eq. (5.49)).

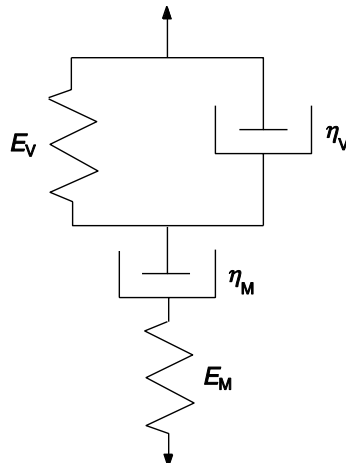
(b) A maximum in the loss modulus plotted as a function of frequency occurs at $\omega = 1/\tau$.

5.5 Given the four-element model illustrated below, derive an analytical solution for the strain behavior and sketch $\varepsilon(t)$ versus time under the following stress conditions:

$$t < 0 \quad \sigma = 0$$

$$0 \leq t < t_1 \quad \sigma = \sigma_o \quad (\text{creep})$$

$$t_1 \leq t < t_2 \quad \sigma = 0 \quad (\text{creep recovery})$$



5.6 In the case of the expression for the dielectric loss constant given by eq. (5.112), the relaxation time can be assigned a temperature dependence of the form

$$\tau = \tau_o \exp(H/RT)$$

where H is the activation energy. If ε'' assumes its maximum value at that temperature (T_{\max}) where $\omega = 1/\tau$, how can the value of H be determined given data in the form of a plot of ε'' versus T at different frequencies, f ?

5.7 Calculate the WLF shift factor, a_T , for polystyrene (PS) at 150°C given that the reference temperature is taken to be the T_g of PS, 100°C, and using (a) the “universal” values of the WLF parameters, C_1 and C_2 , and (b) the reported values of $C_1 = 13.7$ and $C_2 = 50.0$ K for PS.

5.8 If the maximum in the α -loss modulus of polystyrene at 1 Hz occurs at 373 K, at what temperature would the maximum occur at 110 Hz if the activation energy for this relaxation is 840 kJ mol⁻¹?

5.9 (a) Calculate the relaxation modulus, in SI units of GPa, at 10 seconds after a stress has been applied to three Maxwell elements linked in parallel using the following model parameters:

$$E_1 = 0.1 \text{ GPa} \quad \tau_1 = 10 \text{ s}$$

$$E_2 = 1.0 \text{ GPa} \quad \tau_2 = 20 \text{ s}$$

$$E_3 = 10 \text{ GPa} \quad \tau_3 = 30 \text{ s}$$

(b) Does this model give a realistic representation of stress relaxation behavior of a real polymer? Explain.

5.10 An elastomeric cube, 2 cm on a side, is compressed to 95% of its original length by applying a mass of 5 kg. What force is required to stretch a strip of the same elastomer by 50%? The initial length of the strip is 2 cm and its original cross-sectional area is 1 cm².

5.11 If the stress at 23°C of an ideal rubber is 100 psi when stretched to twice its original length, what would be the stress at a 50% extension?

5.12 The length of an ideal rubber band is increased 100% to 12.0 cm at 23°C. Stress on this rubber band increases by 0.2 MPa when it is heated to 30°C at 100% elongation. What is its tensile modulus in MPa at 23°C when it is stretched 2%?

5.13 Calculate the shear modulus (GPa) of a polymer sample in a torsion pendulum with a period of 1.0 s. The specimen is 10 cm long, 2 cm wide, and 7.5 mm thick and the moment of inertia is 5000 g cm².

5.14 For a two-phase system for which the complex shear modulus follows a log rule of mixtures, show that

$$\frac{G''}{G'} \cong \frac{G_1''}{G_1'} \phi_1 + \frac{G_2''}{G_2'} \phi_2.$$

REFERENCES

1. Nielsen, L. E., *Dynamic Mechanical Properties of High Polymers*. SPE Journal, 1960. **16**: p. 525–532.
2. Murayama, T., *Dynamic Mechanical Analysis of Polymeric Material*. 1978, Amsterdam: Elsevier.
3. Gillham, J. K., *Torsional Braid Analysis (TBA) of Polymers*, in *Development in Polymer Characterisation-3*, J. V. Dawkins, ed. 1982, Applied Science Publishers Ltd: London. p. 159–227.
4. Gillham, J. K., S. J. Stadnicki, and Y. Hazony, *Low-Frequency Thermomechanical Spectroscopy of Polymeric Materials: Tactic Poly(methyl methacrylate)*. Journal of Applied Polymer Science, 1977. **21**: p. 401–424.
5. O'Reilly, J. M., H. E. Bair, and F. E. Karasz, *Thermodynamic Properties of Stereoregular Poly(methyl methacrylate)*. Macromolecules, 1982. **15**: p. 1083–1088.
6. Fried, J. R., A. Letton, and W. J. Welsh, *Secondary Relaxation Processes in Bisphenol-A Polysulphone*. Polymer, 1990. **31**: p. 1032–1037.
7. McCrum, N. G., B. E. Read, and H. G. Williams, *Anelastic and Dielectric Effects in Polymeric Solids*. 1967, New York: John Wiley & Sons.
8. Fried, J. R., *Sub-T_g Transitions*, in *Physical Properties of Polymers Handbook*, J.E. Mark, ed. 2007, Springer: New York. p. 217–232.
9. Walters, K., *Rheometry*. 1975, London: Chapman and Hall.
10. Middleman, S., *The Flow of High Polymers*. 1968, New York: Interscience.
11. Matsuoka, S. and Y. Ishida, *Multiple Transitions in Polycarbonate*. Journal of Polymer Science: Part C, 1966. **14**: p. 247–259.
12. Reading, M., *Modulated Differential Scanning Calorimetry—A New Way Forward in Materials Characterization*. Trends in Polymer Science, 1993. **1**(8): p. 248–253.
13. Hutchinson, J. M., *Characterising the Glass Transition and Relaxation Kinetics by Conventional and Temperature-Modulated Differential Scanning Calorimetry*. Thermochimica Acta, 1998. **324**: p. 165–174.
14. Mark, J. E., *Molecular Theories of Rubberlike Elasticity and Some Recent Results on Model Networks and Unusual Fillers*. Kautschuk Gummi Kunststoffe, 1989. **42**(3): p. 191–193.

This page intentionally left blank